

1 **A Multi-site Passive Approach for Studying the Emissions and**  
2 **Evolution of Smoke from Prescribed Fires**

3 Rime El Asmar<sup>1</sup>, Zongrun Li<sup>2</sup>, David J. Tanner<sup>1</sup>, Yongtao Hu<sup>2</sup>, Susan O’Neill<sup>3</sup>, L. Gregory Huey<sup>1</sup>,  
4 M. Talat Odman<sup>2</sup>, Rodney J. Weber<sup>1</sup>

5 <sup>1</sup>School of Earth and Atmospheric Sciences, Georgia Institute of Technology, Atlanta, 30331, USA.

6 <sup>2</sup>School of Civil and Environmental Engineering, Georgia Institute of Technology, Atlanta, 30331, USA.

7 <sup>3</sup>USDA Forest Service, Pacific Northwest Research Station, 400 North 34th Street, Suite 201, Seattle, WA 98103,  
8 USA.

9

10 *Correspondence to:* Rodney J. Weber ([rweber@eas.gatech.edu](mailto:rweber@eas.gatech.edu))

11

12 **Abstract.** We conducted a two-year study utilizing a network of fixed sites with sampling throughout an extended  
13 prescribed burning period to characterize the emissions and evolution of smoke from silvicultural prescribed burning  
14 [at a military base](#) in the southeastern US. The measurement approach and an assessment of instrument performance is  
15 described. Smoke sources, [including those within and off the base](#), are identified, and plume ages are determined to  
16 quantify emissions and study the evolution of smoke PM<sub>2.5</sub> mass, black carbon (BC), and brown carbon (BrC). Over  
17 the 2021 and 2022 prescribed burning seasons (nominally January to May), we identified 64 smoke events based on  
18 high levels of PM<sub>2.5</sub> mass, BC, BrC, and carbon monoxide (CO), of which 61 were linked to a specific burning area.  
19 Smoke transport times were estimated using the mean wind speed along with [the](#) distance between fire and  
20 measurement site, and with HYSPLIT back trajectories. PM<sub>2.5</sub> emission ratios based on  $\Delta\text{PM}_{2.5} \text{ mass}/\Delta\text{CO}$  for fresh  
21 smoke (age  $\leq 1$  hour) ranged between 0.04 and 0.18  $\mu\text{g m}^{-3} \text{ ppb}^{-1}$  with a mean of 0.117  $\mu\text{g m}^{-3} \text{ ppb}^{-1}$  (median of 0.121  
22  $\mu\text{g m}^{-3} \text{ ppb}^{-1}$ ). Both the mean emission ratio and variability were similar to findings from other prescribed fire studies,  
23 but lower than wildfires. Mean emission ratios of BC and BrC were 0.014  $\mu\text{g m}^{-3} \text{ ppb}^{-1}$  and 0.442  $\text{Mm}^{-1} \text{ ppb}^{-1}$   
24 respectively. Ozone enhancements ( $\Delta\text{O}_3$ ) were always observed in plumes detected in the afternoon.  $-\Delta\text{PM}_{2.5}$   
25  $\text{mass}/\Delta\text{CO}$  was observed to increase with plume age in all ozone enhanced plumes suggesting photochemical  
26 secondary aerosol formation. In contrast,  $\Delta\text{BrC}/\Delta\text{CO}$  was not found to vary with plume ages less than 8 hours during  
27 photochemically active periods.

## 28 1. Introduction

29 Large and intense wildfires have been increasing over the past few decades ~~in the US~~ and their emissions are  
30 a critical concern (Singleton et al., 2019; Jaffe et al., 2020). Fire is also an essential ecological process and prescribed  
31 burning, which is the act of starting controlled fires for specific purposes, is an important tool for restoration of  
32 ecosystems, land management, and reducing fuel to prevent destructive wildfires (Kelp et al., 2023). Prescribed fires  
33 are typically conducted during favorable conditions associated with the fuel type and amount, soil moisture, and  
34 meteorology. ~~In~~ For example, in 2018, the [United States Department of Agriculture \(USDA\)](#) Forest Service indicated  
35 a high risk of hazardous wildfires over approximately 234 million acres (~ 95 million ha) of forest lands in the US  
36 (Wyden and Manchin, 2020). However, prescribed fires were conducted over approximately 8.5 million  
37 forestry/rangeland acres (3.4 million ha) in 2018 (Melvin, 2020) ~~federal land management authorities were able to~~  
38 ~~conduct prescribed fires on only approximately 4.6 million acres in 2018, and averaged about 4.1 million acres per~~  
39 ~~year between 2009-2018 (Wise, 2022)~~. The southeastern US has a long history of using prescribed fires (Melvin,  
40 2021), ~~For example, in 2017, 7.6 million acres (3 million ha) out of the 11.3 million acres (4.6 million ha) burned~~  
41 nationally were in the southeast (Melvin, 2018). ~~Each of Florida and Georgia each exceeded 1 million acres (0.4~~  
42 million ha) burned annually (Melvin, 2018). ~~roughly 2.18, 1.26, and 0.94 million acres were burned in 2017 in Florida,~~  
43 ~~Georgia, and Alabama respectively, representing almost two thirds of the prescribed burning conducted nationally (as~~  
44 ~~published by Statista Research Department based on National Interagency Coordination Center in March 20, 2018).~~  
45 ~~The National Interagency Coordination Center estimated that the total prescribed fire acres burned in 2017 nationally~~  
46 ~~was 6.43 million acres~~. Recognizing the need to mitigate the size and severity of wildfires, prescribed burning is  
47 anticipated to increase in the coming years (USDA, 2022).

48 While prescribed burning can be performed under favorable weather conditions, it can still contribute to  
49 serious local and regional air pollution as it is a source of primary and secondary air pollutants (Lee et al., 2008). Like  
50 other types of biomass burning, prescribed burning releases high-large amounts of particulate matter, CO, and  
51 inorganic and organic compounds (Lee et al., 2005), which have negative effects on health and visibility (Bell, 2004;  
52 Huang et al., 2019). Particularly in the southeastern US, prescribed burning was significantly associated with high  
53 PM<sub>2.5</sub> levels (Afrin and Garcia-Menendez, 2020; Larkin et al., 2020). Prescribed fires are often conducted at urban-  
54 rural interfaces creating a buffer zone to prevent the spread of wildfires towards the built environment. However, this  
55 means that the planned fires often occur closer to populated areas, and potentially lead to high population exposure  
56 due to this proximity. Although prescribed fires generally produce less pollutants by consuming less fuel per area  
57 burned than wildfires, the population health costs can be substantially higher for prescribed fires due to burning near  
58 higher population densities (Borchers-Arriagada et al., 2021).

59 Both wildfires and prescribed fires emit a large variety of gases and particulates (Liu et al., 2017b; Burling  
60 et al., 2011; Gkatzelis et al., 2024; Permar et al., 2021; Travis et al., 2023). Gases include nitrogen oxides and volatile  
61 organic compounds that can form ozone and secondary particulate matter. Hazardous air pollutants are also produced  
62 but they may be less detrimental to exposed populations than particulates (O'Dell et al., 2022). PM<sub>2.5</sub>, (particulate  
63 matter with aerodynamic diameter of 2.5 micrometers or smaller), is directly emitted as primary particles and also

64 formed from condensation of emitted gases and their oxidation products, ~~where a major component is secondary~~  
65 ~~organic aerosol (SOA)~~ (Liu et al., 2016; May et al., 2014). While secondary organic aerosol (SOA) can be a significant  
66 component of aged biomass burning PM<sub>2.5</sub>, its contribution changes depending on emissions and atmospheric  
67 conditions. Additionally, the volatile nature of primary and secondary components of PM<sub>2.5</sub> can lead to evaporation  
68 and a net loss in mass as the plume ages. PM<sub>2.5</sub> exposure has been linked in many epidemiological studies to serious  
69 health problems such as respiratory, cardiovascular, and neurological diseases, as well as increased risk of adverse  
70 birth outcomes (Liu et al., 2015; Reid et al., 2016; Naeher et al., 2007; Yu et al., 2023; Xi et al., 2020; Garcia et al.,  
71 2023). Given their significant impact on the environment and health, satellite, airborne, or ground-based studies of  
72 smoke emissions have been extensively conducted.

73 Detection and characterization of wildland fires is an important step towards assessing their impacts. Remote  
74 sensing via satellites can detect wildland fires by thermal anomalies (Kuenzer et al., 2008) or vegetation changes  
75 (Mildrexler et al., 2007). While satellite-based approaches offer valuable insights (Martinsson et al., 2022; Ichoku and  
76 Kaufman, 2005; Christopher et al., 1998), challenges such as cloud cover, spatial resolution limitations, and the  
77 complex nature of fire emissions can hinder accurate detection and quantification of fire impacts, especially for lower-  
78 intensity fires like prescribed burns (Liu et al., 2019; Wang et al., 2018; Martin et al., 2018). Therefore, factors like  
79 Fire Radiative Power (FRP), burned area estimation, and fuel consumption modeling are often integrated into fire  
80 monitoring systems (Li et al., 2020; Nguyen and Wooster, 2020). Satellite-based approaches are highly useful (Ichoku  
81 and Kaufman, 2005; Christopher et al., 1998; Kaufman et al., 1989; Martinsson et al., 2022), but there are limitations,  
82 including temporal coverage and spatial resolution (both horizontal and vertical) (Liu et al., 2019; Ichoku et al., 2016),  
83 detector sensitivity, interferences (e.g., clouds or surface conditions), and interactions between different emissions  
84 (Liu et al., 2019; Wang et al., 2018; Martin et al., 2018). This can lead to significant under-detection of fires and  
85 limitations in quantifying emissions needed to determine population exposures, especially for lower intensity  
86 prescribed fires (Nowell et al., 2018; Larkin et al., 2020; Martin et al., 2018; Buysse et al., 2019; Jaffe et al., 2020).

87 Aircraft (fixed wing and helicopters) and more recently drones are commonly used in airborne studies of  
88 wildland fires (Decker et al., 2021b; Cubison et al., 2011; Aurell and Gullett, 2024) and have been deployed for  
89 prescribed burning studies- (Yokelson et al., 1999; May et al., 2014; Pratt et al., 2011; Aurell et al., 2021). Airborne  
90 studies provide high spatial resolution data that are often used to assess evolution of smoke properties by  
91 measurements at various downwind distances, however, it is non-continuous, and can miss certain aspects of smoke  
92 emissions, such as longer-term smoldering, especially at night (Burling et al., 2011). Employing a combination of  
93 airborne and ground-based measurements can be beneficial in providing a comprehensive view of the plume- (Burling  
94 et al., 2011; Akagi et al., 2014; Yokelson et al., 2013; Strand et al., 2016).

95 In ground-based studies, ~~measurement sites can be mobile or fixed.~~ Mobile labs may capture dynamic air  
96 quality patterns and to some extent assess spatial variability of species distributions in plumes and their changes with  
97 plume age (Levy et al., 2014; Fiddler et al., 2024; Lee et al., 2023). However, they are usually limited in space and  
98 instrumentation capacity, such as filter samples collected only during stationary measurements (Warneke et al., 2023).  
99 Interferences from the power source, vibration and speed changes during transportation can affect instrument stability

100 and performance leading to inaccurate measurements or limiting the type of instruments that can be used. Attempting  
101 to track wildland smoke plumes can be challenging due to unpredictable winds and dispersion conditions combined  
102 with access limitations. For example, Burling et al. reports successfully sampling smoke from 2 out of 14 prescribed  
103 fires using a battery powered mobile FTIR system (Burling et al., 2011).

104 Fixed [ground-based](#) monitoring stations equipped with various instruments provide continuous, localized  
105 measurements for short or long-term monitoring for studies assessing diurnal, seasonal, and long-term trends in air  
106 pollution. Multiple sites provide spatial coverage within a region. A variety of highly sensitive instruments can be  
107 deployed, ensuring accurate and precise measurements of various pollutants that can be compared with air quality data  
108 across different locations for regional assessments (Strand et al., 2016; Warneke et al., 2023). [The importance of pre-](#)  
109 [existing fixed monitoring sites lies in their ability to capture wildfire smoke events that can occur at any time](#)  
110 (Selimovic et al., 2019; Jaffe et al., 2022). [These sites often include regulatory monitoring stations, which are highly](#)  
111 [valuable for studying local and regional smoke impacts over both short and long-term periods. For example, Jaffe et](#)  
112 [al. used PM<sub>2.5</sub> and CO observations from a regulatory monitoring site in Sparks, NV, collected from May to September](#)  
113 [between 2018 and 2021, as indicators of wildfire smoke in urban areas](#) (Jaffe et al., 2022). [Investigating emissions](#)  
114 [and evolution of prescribed fires based on fixed sites is not as common, and there are limitations with this approach,](#)  
115 [but also some advantages.](#)

116 ~~The overall goal of this study was to investigate the emissions and evolution of~~  
117 ~~prescribed fires and to provide data to test model simulations. Results~~ from a two-year study utilizing fixed monitoring  
118 stations and continuous sampling in a region of active prescribed burning [at Fort Moore in central Georgia, USA](#)  
119 ~~are presented.~~ The observations are analyzed to [identify smoke plumes and determine their sources, such as those set](#)  
120 [within the Fort or from burning in surrounding areas. We also use these data to estimate the age of the smoke detected](#)  
121 ~~to determine emission ratios and changes with plume age~~ ~~determine emission ratios~~ of PM<sub>2.5</sub> mass, BC, and BrC and  
122 their variability. Not all smoke from the prescribed fires ~~set within the Fort are in the region is~~ detected so the overall  
123 impact of all fires on regional air quality cannot be determined and is better addressed by a model simulation. Instead,  
124 our goal is to sample multiple smoke events so that an analysis of the data will provide a robust characterization of  
125 smoke from prescribed burning [within the Fort and](#) in the region and sufficient data ~~to test model simulations.~~ [to](#)  
126 [evaluate ground-level pollutant concentrations predicted by “smoke” models in prescribed fire simulations. Our](#)  
127 [concentration data cover measurements over a large range of distances from the burn plots. Fresh plume measurements](#)  
128 [with ages less than 1 hour can be used in evaluating the predictions of local scale models such as the Wildland urban](#)  
129 [interface Fire Dynamics Simulator \(WFDS\) \(Mell et al., 2007\) and the QUIC-Fire \(Linn et al., 2020\). They can also](#)  
130 [be used in evaluating the emissions and plume-rise parameterizations of larger scale models like the BlueSky](#)  
131 [framework \(Larkin et al., 2009\). Additionally, more aged smoke measurements can be used to test the predictions of](#)  
132 [downwind concentrations in coupled fire-atmosphere models such as WRF-SFIRE \(Mandel et al., 2011\) as well as](#)  
133 [chemical transport models like the Community Multiscale Air Quality \(CMAQ\) model \(Appel et al., 2021\), when they](#)  
134 [are equipped with fire plume parameterizations.](#) In the following sections, we describe the methodology, data analysis  
135 approach, case studies ~~on~~ [of](#) various detected or missed smoke plumes [so that attribution of smoke from fires within](#)

136 ~~the Fort can be assessed, and initial findings~~ on emission estimates of PM<sub>2.5</sub> mass, BC, and BrC and their evolution  
137 ~~are compared to other prescribed and wildfire studies.~~ These findings ~~are can help needed~~ to assess the impact of  
138 prescribed burns ~~by a specific entity or organization~~ on a variety of public health and policy issues.

## 139 2. Method

### 140 2.1. Site description

141 Prescribed burning at Fort Moore Army Base, (formerly Fort Benning), in west central Georgia, United  
142 States, was studied during March through May of 2021 and February through May of 2022. Since 1981, prescribed  
143 burning has been used as a land management tool at the 182,000 acres (~ 74,000 ha) military base, of which 145,000  
144 acres (~ 59,000 ha) are forested lands. Vegetation is characterized by pine-dominated uplands, and hardwood-  
145 dominated bottomlands, with the dominant tree species being longleaf pine and white oak, respectively. Unintended  
146 Small wildfires ignited during military training exercises also occur at the base and the land managers have been  
147 recording data on both prescribed fires and wildfires since the 1980s. Prescribed burning at the Fort has been effective;  
148 it has reduced the frequency of wildfires from ~ 300-500 wildfires/year in the early 1980s to less than 100  
149 wildfires/year in the mid-1990s. During this period the prescribed fire burnt area changed from ~7,500 acres (~ 3,000  
150 ha) in 1981 to ~ 12,000 acres (~ 5,000 ha) in 1992. Currently, 30,000 woodland acres (~ 12,000 ha) are burned annually  
151 using controlled fires, with a future planned burning of 45,000 acres (~ 18,000 ha) annually. Prescribed burning on  
152 the Fort is also used for ecological objectives, such as restoring the longleaf pine forest and creating and maintaining  
153 habitat for red-cockaded woodpeckers. Prescribed burning occurs from December through May when there is  
154 sufficient but not excessive rainfall, and suitable temperatures and wind conditions to burn deadwood, brush, and low-  
155 growing vegetation accumulating on the forest floor. The area of the base is divided into 332 burn units that range in  
156 size from 100 to 1,800 acres (~ 40 to 728 ha) and are burnt alternately every two to three years.

### 157 2.2. Measuring sites

158 One instrumented research trailer (7'W x 18'L x 6.5'H) was deployed in the 2021 burning season (March 18,  
159 2021 to May 15, 2021), and successively trailers (6'W x 12'L x 7'H) were added in 2022 (February 11, 2022 to May  
160 18, 2022) reaching a total of five trailers located at different sites throughout the Fort. In 2021, the one trailer operated  
161 at the same location until it was moved on April 26, 2021 to a new site for the remaining season as expected burning  
162 regions at the Fort changed. The trailers sampled continuously, except during periods of power loss or technical issues.  
163 The locations of trailers, shown in Fig. 1, were chosen based on power availability, prevailing wind, and burning plans  
164 set prior to the burning season.

### 166 2.3. Instrumentation

167 To characterize the prescribed fire smoke, the trailers were equipped with several instruments selected based  
168 on factors such as availability, ability for extended stand-alone operation, and their significance to the study. All  
169 sampling was done through inlets nominally 4 m above ground level and 1.5 m above the trailer roof.

170 Measurements included, carbon monoxide (CO), nitrogen oxides (NO, NO<sub>2</sub>, NO<sub>x</sub>), ozone (O<sub>3</sub>), PM<sub>2.5</sub> mass  
171 concentration and black carbon (BC) concentration and brown carbon (BrC) light absorption coefficients. Carbon  
172 monoxide- serves as a standard tracer for combustion sources in atmospheric chemistry studies since it is a relatively  
173 long-lived species, with a typical lifetime of ~ 1 month, emitted during incomplete combustion and used as a~~smoke~~  
174 tracer ~~of to track smoke's~~ movement and dispersion (Forrister et al., 2015; Liu et al., 2016). Other forms of incomplete  
175 combustion emissions (e.g., mobile sources) and oxidation of VOCs are also CO sources. CO mixing ratios were  
176 measured by IR analyzers (Thermo Fisher Scientific Inc, model 48C, Franklin, MA) with a lower detection limit  
177 (LOD) of 0.04 ppm at an averaging time of 390 seconds. The measurements alternated between blank and ambient  
178 measurements every 195 seconds. The blanks were determined with a custom-built CO scrubber made of 0.5 % Pd on  
179 alumina catalyst heated to 180 °C (Parrish et al., 1994), which oxidizes CO to CO<sub>2</sub>. Calibration of CO analyzers was  
180 performed at 2.2 ppm concentration before and after each field study using a 100 ppm CO in air standard purchased  
181 from nexAir (Memphis, TN).

182 O<sub>3</sub> was measured using an ultraviolet (UV) photometric analyzer (Thermo Fisher Scientific Inc, model 49C,  
183 Franklin, MA) zeroed through an O<sub>3</sub> scrubber in the instrument, with LOD of 1.0 ppb and averaging time of 20  
184 seconds. The analyzer was calibrated before and after each field deployment using an O<sub>3</sub> calibrator (Thermo Fisher  
185 Scientific Inc, model 49C, Franklin, MA). We note that O<sub>3</sub> may be overestimated due to interferences from VOCs  
186 emitted by the fire (Long et al., 2021), but the instrument used has been found to be in agreement with a federal  
187 reference method (Gao and Jaffe, 2017). NO<sub>x</sub> species were measured using a chemiluminescence NO-NO<sub>2</sub>-NO<sub>x</sub>  
188 analyzer (Thermo Fisher Scientific Inc, model 42i, Franklin, MA). The NO<sub>x</sub> analyzer was calibrated automatically  
189 every 6 hours, using NO and NO<sub>2</sub> calibration standards purchased from Airgas (Radnor, PA) and has an LOD of 0.40  
190 ppb.

191 PM<sub>2.5</sub> mass concentration was determined with a Tapered Element Oscillating Microbalance (TEOM) series  
192 1400a ambient particulate monitor (Thermo Fisher Scientific, Franklin, MA) with data recorded at an averaging time  
193 of 60 seconds and typical detection limit of 5.58 µg m<sup>-3</sup> determined by 3 standard deviations of blank (filtered ambient  
194 air) measurements. This data was subsequently averaged to time intervals of 20 and 60 minutes to mitigate noise,  
195 especially when sampling under background conditions. The TEOM series 1400a developed originally by Rupprecht  
196 & Patashnick is a US-EPA approved instrument for measuring the mass concentration of ambient PM<sub>2.5</sub> and PM<sub>10</sub> and  
197 could be used for Federal Equivalent Method (FEM) regulatory measurements (Liu et al., 2017a; Patashnick and  
198 Rupprecht, 1991). It is a gravimetric measurement that determines the mass accumulated on a microbalance over a  
199 specified time interval at a monitored sample air flow rate. The sample air is preconditioned to a temperature of 50 °C  
200 to remove liquid water interferences (Patashnick and Rupprecht, 1991), which may lead to the evaporation of highly  
201 volatile PM<sub>2.5</sub> components, potentially underestimating the total mass concentration. -Mass concentration over an  
202 averaging period is calculated from the difference recorded between successive intervals. Due to random fluctuations

203 in the instrument operation when concentrations are low, this can lead to negative numbers, illustrated by the frequency  
204 distribution of high time resolution data recorded by one TEOM shown in Fig. S1. When determining the average  
205 background concentration, we include the negative mass concentrations since converting negative concentrations to  
206 one half the LOD or ignoring them will produce an average that is biased high. In 2021, PM<sub>10</sub> TEOMs were also  
207 deployed but this was found to be highly influenced by pollen, which can be high in the springtime, and so the  
208 measurement was discontinued. Regional hourly PM<sub>2.5</sub> mass was reported at two Environmental Protection Division  
209 (EPD) sites. In the following analysis we compare the PM<sub>2.5</sub> measured within the Fort to the EPD measurements at  
210 the Columbus Airport and Phenix City South Girard (PCSG) school shown on the map in Fig. 1a. At Columbus  
211 Airport, the Teledyne T640, which is based on broadband spectroscopy, is used, while the Met One BAM-1022 mass  
212 monitor is used in Phenix City, utilizing a beta attenuation technique.

213 PM<sub>2.5</sub> black carbon (BC) mass concentration was measured by aethalometers. A range of multi and single  
214 wavelength instruments were deployed. Two were seven wavelength instruments (Magee Scientific, model AE33 and  
215 model AE31, Berkeley, CA) with detection ranges of 0.1–100 µg m<sup>-3</sup> and averaging times of 60 and 120 seconds  
216 respectively, one 2-wavelength aethalometer (Magee Scientific, model AE22, Berkeley, CA) of 0.1 µg m<sup>-3</sup> detection  
217 limit and 60 seconds averaging time, and two single wavelength particle soot absorption photometers (PSAPs)  
218 (Radiance Research, Seattle, WA) of sensitivity > 0.1 µg m<sup>-3</sup> for 60 seconds averaging time. For the multiwavelength  
219 aethalometers, BC was determined from the light absorption at 880 nm using the manufacturer's specified mass  
220 absorption cross-section (MAC) of 7.77 m<sup>2</sup> g<sup>-1</sup>, whereas for the single wavelength PSAPs, BC was determined from  
221 the optical absorption coefficient at 565 nm assuming a specific mass absorption cross-section of 10 m<sup>2</sup> g<sup>-1</sup> following  
222 the manufacturer's specifications. Two spot samplings of the model AE33 corrected for mass loading errors. This was  
223 not done in the other instruments and so the data of the aethalometers (AE31 and AE22) were corrected for loading  
224 interference using the method of Virkkula et al. (Virkkula et al., 2007). PSAPs measurements were not corrected due  
225 to unavailability of scattering coefficients needed for correcting filter-based PSAP measurements (Bond et al., 1999;  
226 Virkkula et al., 2005), which may lead to 10-20% underestimation of BC at sites where PSAPs were installed.

227 Brown carbon (BrC) was calculated from the 7-wavelength aethalometer measurements. BrC is largely  
228 produced from biomass burning (Hecobian et al., 2010; Laskin et al., 2015; Yan et al., 2018; Fleming et al., 2020) and  
229 in the following analysis used as a unique indicator of biomass burning smoke. While a small amount of BrC can be  
230 produced from mobile sources and other sources of incomplete combustion, in the US, its predominant source is  
231 biomass burning (Jo et al., 2016; Hecobian et al., 2010). We calculate the light absorption of BrC at 365 nm as a  
232 marker for BrC levels. Using the aethalometer data, the absorption coefficient, which corresponds to (BC+BrC), was  
233 inferred by multiplying mass concentration at each wavelength by the corresponding MAC value provided by the  
234 manufacturer (Magee Scientific, Berkeley, CA).  
235 The absorption coefficient at 365 nm was determined by extrapolating the linear regression of log absorption  
236 coefficient vs log wavelength since the lowest wavelength at which the aethalometer operates is 370 nm. The slope of  
237 the linear relationship represents the negative of the absorption Angstrom Exponent (AAE), a parameter used to study  
238 the optical properties of the aerosol. BrC at 365 nm was then calculated by removing the estimated contribution of BC



239 at 365 nm assuming that BrC does not absorb at 880 nm and that AAE of pure BC is 1. BrC absorption at shorter  
240 wavelengths is the difference of aethalometer-measured total absorption and the extrapolated BC absorption (Lack  
241 and Langridge, 2013). All data of the light absorption of BrC discussed in this work corresponds to the absorption  
242 calculated at 365 nm. Both  $AAE_{total}$  and  $AAE_{BrC}$  were calculated as the negative slopes of log absorption coefficient  
243 of total (BC+BrC) and BrC respectively, as a function of log wavelengths. For  $AAE_{total}$  the fit included wavelengths  
244 370–880 nm (i.e., 370, 470, 520, 590, 660, 880), whereas for  $AAE_{BrC}$  the wavelengths ranged from 370 to 660nm (i.e.,  
245 370, 470, 520, 590, 660).

246 In our analysis, we used meteorological and fuel moisture data from the Remote Automated Weather  
247 Stations (RAWS) available online (<https://raws.dri.edu/index.html>). ~~located at the base in our analysis,~~ The closest  
248 RAWS weather station to all sites is named Ft. Benning Georgia (~~shown in~~ Fig. 1a). In each trailer, all instruments  
249 were connected to a laptop computer with remote access to reduce personnel time spent at the sites. Sites were  
250 generally visited every 1 to 2 weeks during which regular instrument checks and maintenance were performed, such  
251 as restoring power, changing filters (for TEOMs and PSAPs), measuring and recording flow rates and other instrument  
252 performance parameters.

## 253 **2.4. Tools and analysis methods**

### 254 **2.4.1 Normalized Excess Mixing Ratios:**

255 To account for dilution of species of interest in a smoke plume, Normalized Excess Mixing Ratios (NEMRs)  
256 are used. The NEMR is the ratio of enhancement of a studied species above the local background concentrations to  
257 the enhancement of a long-lived component co-emitted from the biomass burning event. CO is often used as the  
258 reference species, i.e., NEMR of species X is  $\Delta X/\Delta Y$ , where Y is CO measured in the same sample as X. To determine  
259 the NEMR of X and the contribution of smoke to X from an identified burning region, the background concentration  
260 of X (i.e., concentration if no smoke emissions) is subtracted from the measurement. In our study we used the average  
261 of the measurements before and after the smoke event as the background since sampling was not performed upwind  
262 of the fire. This method is supported by the observation from multiple sampling sites of spatially uniform background  
263 concentrations and, in most cases, very low background concentrations relative to those recorded in the smoke.  
264 However, there is more uncertainty when calculating O<sub>3</sub> NEMRs due to significant levels and diurnal changes in  
265 background concentrations. NEMRs can also be determined from the slope of linear regressions. Here, we determine  
266 NEMRs in each smoke event for PM<sub>2.5</sub> mass, BC, and BrC normalized by CO by first removing background  
267 concentrations for data recorded during the event and then calculating the slope by linear regressions (i.e., the slope  
268 of PM<sub>2.5</sub> mass concentration, BC concentration, or BrC absorption at 365 nm versus CO concentrations to determine  
269 the respective NEMRs).

### 270 **2.4.2 Determining Smoke Sources and Plume Age:**

271 To match specific fires to observed smoke at the monitoring sites, several methods were used. Data from the  
272 Fire Information for Resource Management System (FIRMS) provided active fire data based on thermal anomalies.

273 [These are based on measurements from the Moderate Resolution Imaging Spectroradiometer \(MODIS\), carried by](#)  
274 [Aqua and Terra satellites, and the Visible Infrared Imaging Radiometer Suite \(VIIRS\), carried by the Suomi National](#)  
275 [Polar-orbiting Partnership \(Suomi NPP\) and NOAA-20 satellites. FIRMS provides live and historical fire maps and](#)  
276 [data that can be accessed online \(<https://firms.modaps.eosdis.nasa.gov/>\). This platform can be used to pinpoint specific](#)  
277 [locations and obtain distances between points, which is useful for identifying possible fires where smoke was](#)  
278 [transported to the sampling site and the time for smoke transport when combined with wind speed and direction data.](#)  
279 [Although the FIRMS fire map is updated every 5 minutes, the polar orbiting satellites pass over the location only](#)  
280 [twice per day meaning that some fires starting and ending between satellite observations are not detected \(Schroeder](#)  
281 [and Giglio, 2018; Giglio et al., 2021\). Also, small or relatively cool fires may not be detected, especially when there](#)  
282 [is significant cloud coverage, or thick smoke, or a continuous, thick forest canopy, which can block satellite detection](#)  
283 [of prescribed understory burns in forests. Cloud coverage data are available online](#)  
284 [\(<https://worldview.earthdata.nasa.gov>\) and satellite data, including MODIS/VIIRS overpass times, the number of](#)  
285 [active fire detections per pass, and FRP for all fires that impacted the monitoring sites, can be downloaded from the](#)  
286 [abovementioned FIRMS website. Burn data provided by Fort Moore were used with the FIRMS data to minimize](#)  
287 [limitations with each method for identifying sources of observed smoke. For each of the 64 smoke events studied in](#)  
288 [the paper, burn data are added to the supplementary material \(Table S1\). Additionally, temperature, relative humidity,](#)  
289 [and fuel moisture data used can be accessed online through RAWS USA Climate Archive](#)  
290 [\(<https://raws.dri.edu/index.html>\) at the closest to all sites weather station named Ft. Benning, Georgia.](#)

291 [The Hybrid Single-Particle Lagrangian Integrated Trajectory \(HYSPLIT\) model \(Stein et al., 2015\) was used](#)  
292 [to calculate back trajectories from monitoring sites. This trajectory analysis was based on meteorological data derived](#)  
293 [from the Weather Research and Forecasting \(WRF\) model \(Shamarock et al., 2019\) enhanced with grid nudging and](#)  
294 [observational nudging \(Deng et al., 2009; Liu et al., 2005\), using a 20-minute timestep. The WRF domain settings are](#)  
295 [shown in Fig. S2. The winds used in the trajectory analysis are from the 1-km grid resolution domain. Each analysis](#)  
296 [covered a total of 10 trajectories, all below the planetary boundary layer \(PBL\). HYSPLIT was run with 10-minute](#)  
297 [timesteps, and the locations of fires were determined based on FIRMS data and the Fort Moore Fire Management](#)  
298 [records.](#)

### 299 **3. Results and discussion**

#### 300 **3.1. Assessment of PM<sub>2.5</sub> monitors and background concentrations**

301 [The focus of this analysis is on PM<sub>2.5</sub> mass concentrations from the prescribed fires. Aerosol particle mass](#)  
302 [concentrations measurements are difficult, especially at background conditions when concentrations are low.](#)  
303 [Calibrating instruments with known mass standards is also problematic. We performed intercomparisons between](#)  
304 [monitors including direct comparisons for two pairs \(side-by-side\) and intercomparison of background PM<sub>2.5</sub> mass](#)  
305 [concentrations measured by the study TEOMs to the values reported at state monitoring sites. For example, two](#)  
306 [TEOMs \(used in main and T1293 trailers\) collocated at Eglin Air Force Base in 2023 from March 19, 2023 at 8:00](#)  
307 [till March 20, 2023 at 10:00, had an orthogonal regression slope of  \$0.98 \pm 0.09\$ , intercept of  \$0.45 \pm 0.37 \mu\text{g m}^{-3}\$  and  \$r^2\$](#)

of 0.84 (see Fig. S3). The main trailer TEOM was also compared with the TEOM used on T1291 when they were collocated at the Georgia Institute of Technology from September 22, 2023 at 19:00 till October 07, 2023 at 14:00. Although measurement during that period was close to background levels, the comparison resulted in an orthogonal regression slope of  $0.88 \pm 0.03$ , intercept of  $3.75 \pm 0.09 \mu\text{g m}^{-3}$  and an  $r^2$  of 0.76 (see Fig. S4). The frequency distribution used to determine the mean values, and mean background values of the data recorded at the main trailer and the EPD sites in 2022 are shown in Fig. S5. The mean concentrations in 2022 were 7.02, 9.47, 9.01, 9.26, and  $7.11 \mu\text{g m}^{-3}$  at the main trailer, T1293, T1292, T1921, and T1290 respectively and 10.33 and  $10.67 \mu\text{g m}^{-3}$  at the Columbus Airport and PCSG school EPD sites respectively. Background air  $\text{PM}_{2.5}$  mass concentrations were also determined by excluding smoke events (discussed below). The monthly backgrounds of  $\text{PM}_{2.5}$  mass concentrations are shown in Table S24. Background concentrations were in the range of approximately  $3\text{--}7 \mu\text{g m}^{-3}$  for monitors at the Fort, and between 7 and  $9 \mu\text{g m}^{-3}$  at the state monitoring sites (Table S32). Higher background  $\text{PM}_{2.5}$  mass concentrations at the state sites are likely due to the local anthropogenic (urban) influence. These comparisons provide confidence in the mass measurements that cannot be calibrated in a manner similar to gas monitors.

Background concentrations of CO and BC are also given in Table S24. Background CO ranged between  $\sim 150$  and  $200$  ppb and background BC ranged between  $0.14$  and  $0.57 \mu\text{g m}^{-3}$ . In terms of spatial variation within Fort Moore, background levels of measured species were slightly lower in sites located far from the main roads and training areas, such as measurements at the main trailer during May of 2021 and the entire 2022 season. No significant temporal variation is observed, although fires within and in the vicinity of the base increase during the transition from winter to spring, indicating that smoke was efficiently dispersed on time scales of approximately one day. Frequent smoke events where concentrations of the various measured species were substantially above these background levels were observed during the 2021 and 2022 field deployments.

## **3.2. Study of fires at Fort Moore during 2021 and 2022**

### **3.2.1 Overview of the Smoke Detected**

We first present an overview of the measurements at Fort Moore during two burning seasons. In the 2021 season, only one research (main) trailer was deployed. In the following year, four more were deployed for a total of five sites.

On March 18, 2021, a fully equipped trailer was deployed in the Northern boundary of Fort Moore, and we sampled at that location until April 26, 2021. It was then moved to the center of the Fort for sampling from April 26 to May 15, 2021 (see Fig. 1a). During this period, peaks of measured species were observed, as shown in the time series of  $\text{PM}_{2.5}$  mass in Fig. 2b. A peak of a measured species is defined as the highest value observed within the data points, spanning from an initial rise until a return to background levels. Maximum  $\text{PM}_{2.5}$  mass concentrations reached  $2000 \mu\text{g m}^{-3}$  for 20-minute averaged data and  $1400 \mu\text{g m}^{-3}$  for hourly-averaged data (Table S43). A total of 11  $\text{PM}_{2.5}$  peaks with mass concentrations greater than  $35 \mu\text{g m}^{-3}$  were recorded. In 2022, over the course of the entire burning season, 32 days recorded a total of 53  $\text{PM}_{2.5}$  mass concentration peaks greater than  $35 \mu\text{g m}^{-3}$  were detected across the five measuring sites, as shown in Fig. 2c with similar high concentrations, reaching  $841 \mu\text{g m}^{-3}$  for 20-minute averaged and  $513 \mu\text{g m}^{-3}$  for hourly-averaged data (Tables S54 to S87).

344 ~~We focus on the larger smoke plumes with higher PM<sub>2.5</sub> mass concentrations~~ to identify their sources and  
345 estimate the emissions and evolution of PM<sub>2.5</sub> mass because the burning areas are readily identified (e.g., detected  
346 remotely by satellite) and the plume can be easily delineated from the background. An increase in measured species  
347 is considered a peak, or event, when the 20-minute average PM<sub>2.5</sub> mass is greater than 35 µg m<sup>-3</sup> and the 40-minute  
348 average PM<sub>2.5</sub> mass concentration (average of two consecutive measurements) is larger than 30 µg m<sup>-3</sup>. This excludes  
349 shorter transient events that includes a passing vehicle that can occur at measuring sites near training areas.

350 The large peaks in PM<sub>2.5</sub> mass are always accompanied by an increase in CO, BC, and BrC. Figure 3 shows  
351 the scatter plots of 20-minute averaged data collected in 2021 and 2022. The linear relation between PM<sub>2.5</sub> and CO,  
352 BC, and BrC during events resulted in an r<sup>2</sup> of 0.85, 0.68, and 0.71 respectively. ~~On the other hand, for non-events~~  
353 ~~data, which include all observations during the entirety of the measurement period, r<sup>2</sup> drops to 0.12, 0.33, and 0.17 for~~  
354 ~~PM<sub>2.5</sub> mass vs CO, BC, and BrC respectively.~~ These correlations suggest that the events identified correspond to  
355 periods of measuring smoke from biomass burning sources. However, it is important to note that variability still exists  
356 in slopes among different events, which will be explored and discussed in later sections.

### 357 **2.4.3.3. Determining smoke sources**

358 ~~When a smoke plume is identified the goal is to link it to a specific burn area and determine the transport~~  
359 ~~time. To study the emission and evolution of smoke plumes and make our measurements useful for evaluating smoke~~  
360 ~~transport and dispersion models, we aim to link identified smoke plumes to specific burn areas and determine their~~  
361 ~~transport time. Attribution of the smoke to specific fires is also useful for assessing the impacts of a specific prescribed~~  
362 ~~burning program, such as the one at Fort Moore.~~ Identifying the location of prescribed fires was complicated by several  
363 factors. In this study, we had limited beforehand information on the timing and location of planned burns ~~from the~~  
364 ~~burn managers.~~ Moreover, smoke from other sources, such as prescribed and wildfires in the region, but not within  
365 the Fort, as well as uncertainty and variability in wind patterns at the time of burning, led us to utilize multiple methods  
366 to determine the source of each identified smoke episode.

367 Our analysis started by using satellite data from FIRMS to identify locations of fires (when the satellite passed  
368 overhead). After the end of the study, those locations were verified by cross-referencing with the [Fort Moore](#) fire  
369 management reports, which provided locations and acreage of prescribed burns and ongoing wildfires exclusively  
370 within the Fort for each day. Afterwards, we pinpointed the source of smoke that reached the monitors by averaging  
371 the wind vectors at and before the peaks using the meteorological data from RAWS. This provided the expected  
372 general upwind region the smoke likely came from. We also used the HYSPLIT model to conduct back trajectory  
373 analysis from the measurement trailer for 8 hours prior to ascertain if the air mass containing the measured smoke had  
374 passed the satellite-identified hot spot or the units reported as burnt by the Fort's Fire Management. HYSPLIT initial  
375 altitudes were determined by the PBL height, where trajectories for 10 equally distributed altitudes between 10 m  
376 above the surface and the top of the PBL were generated for each simulation. For example, if the PBL height was 100  
377 m, trajectories were calculated at 10, 20, 30, 40, 50, 60, 70, 80, 90, and 100 m.

378 Through the systematic combination of these methods, we attempted to identify specific fire sources  
379 associated with each observed smoke event and the time of transport of the smoke from the fire to the measurement

380 site (referred to as smoke age). This procedure was successful for 61 out of 64 of the identified smoke events. We  
381 failed to identify 3 events that had no apparent source in agreement with the studied wind patterns. Moreover, of the  
382 61 identified smoke events, 7 events were matched to different sources using the observed wind vector method versus  
383 using the HYSPLIT trajectories, 7 events were matched to sources using HYSPLIT only, and 5 events were matched  
384 to sources using wind vector method only.

385 The variability of smoke sources determined in some cases is attributed to the difference between wind  
386 direction used by HYSPLIT and that recorded by RAWS used for the wind vector calculation. In HYSPLIT, wind  
387 data are derived from the three-dimensional wind fields predicted by the application of the WRF model. Figure 4  
388 shows a comparison between modeled and observed wind direction during the events identified in 2021 and 2022 at  
389 the main trailer. A closer alignment in wind direction is observed during higher-speed wind conditions.

390 As an example of source determination, Figure 5a shows the time series of CO, PM<sub>2.5</sub> mass, BC, and BrC  
391 during three smoke episodes recorded on April 6, 7, and 8, 2021, which are indicated by blue, yellow, and green  
392 shading, respectively. Along the top of the graph are the hourly averaged wind vectors based on data from RAWS.  
393 Note the high correlation between PM<sub>2.5</sub> mass and CO concentration and BrC absorption coefficient indicating that  
394 the PM<sub>2.5</sub> peaks were due to smoke. During those three days, the three events were measured during late evening,  
395 nighttime, and early morning periods. In each case, there is a time delay between when the burning occurred and when  
396 the plume was measured, due to the transport time. In all three cases, burning regions at the Fort were identified as  
397 the source. Consider the first smoke event detected at the trailer between 1:00 and 11:00 on April 6, 2021 (blue shaded  
398 region in Fig. 5a). Figure 5b shows the map of the Fort and FIRMS satellite data on the day before (April 5, 2021)  
399 indicating 2 hot spots on the base, which were later verified in the fire report as burning of 2 units and 4 sections of a  
400 third unit. Both burns were to the south and south-southeast of the trailer, and the winds were from the  
401 ~~westerly, northwest, west, and southwest~~ during the daytime on April 5, 2021. By midnight, the wind direction shifted,  
402 with air flowing from the south and the southeast, transporting smoke to the trailer's location, leading to elevated  
403 concentrations of species on monitors. Wind speeds were very low at night. At about 8:00, wind speed increased, its  
404 direction changed, and concentrations of the species all dropped.

405 Burning of other units took place on April 6, 2021 at distances 0.8, 2.1, 2.5, 6.3, and 7.2 miles from the trailer.  
406 The level of measured smoke products started increasing in the evening after the winds became southwesterly and  
407 stayed high until the morning of the next day (April 7, 2021) (yellow shaded region in Fig. 5a). Later at night of April  
408 7 (green shaded region in Fig. 5a), concentration levels increased slightly after the burning of two connected units to  
409 the south of the base during the daytime of April 7, 2021 at a distance ranging between 10.8 and 12.5 miles as indicated  
410 by the Fort's Fire Management and seen on FIRMS. HYSPLIT back trajectory analysis, shown in Fig. 5 (e, f, and g),  
411 was conducted for assessing our conclusion on the sources, especially in cases of wind variation and/or multiple fires  
412 such as for the peaks monitored on April 6 (blue shaded region in Fig. 5a) and April 7, 2021 (yellow shaded region in  
413 Fig. 5a). Since there are multiple fires on the Fort all in the same southern direction relative to the trailer, the exact  
414 source cannot be determined solely based on wind vectors from RAWS data. In these cases, HYSPLIT back  
415 trajectories help to pinpoint the exact fire or fires contributing to the smoke event observed. In both cases on April 6

416 (blue shaded region in Fig. 5a) and April 7, 2021 (yellow shaded region in Fig. 5a), the closer fire was the source of  
417 smoke as shown in Fig. 5e and 5f.

#### 418 2.5.3.4. Determining smoke age

419 ~~The~~ An estimate of the smoke age is needed to separate fresh from aged smoke to estimate emissions of  
420 various species (i.e., in fresh smoke) and the changes in their concentrations with plume age. The physical age of  
421 smoke is the time it takes the smoke to be transported from the source to the monitoring sites. Following the concept  
422 presented for source identification, the transport time of smoke is estimated by averaging wind speed over the period  
423 it takes for the smoke to travel from the fire to the measurements sites, determined by iteration (mean wind speed  
424 recalculated with new transport time, until convergence). When the average wind speed in the hour leading up to the  
425 peak does not result in a smoke age of one hour or less, we begin iterative steps by calculating the average wind vector  
426 for additional one hour increments at a time. A detailed example on using average wind vector in estimating the  
427 physical age of smoke is provided in the Supplemental section S.1. It is important to note the uncertainty in the  
428 estimated smoke age using this method for smoke monitored before and after the peak (maximum concentration),  
429 particularly when the smoke event duration (from the start to the end of smoke monitoring) is prolonged, and when  
430 wind conditions are highly variable. The age was also determined from the HYSPLIT back trajectories as the time  
431 when the lowest trajectory intersects the source of smoke identified. The backward trajectory is initiated from the start  
432 time of the smoke event. Due to uncertainties in the WRF simulated winds, particularly at night when wind speeds are  
433 low, the backward trajectory occasionally missed the source. Therefore, a series of HYSPLIT simulations with 20-  
434 minute intervals from the event start time until the source of smoke could be identified were conducted. The 20-minute  
435 interval was chosen based on the temporal resolution of the WRF data.

436 For the three events discussed in Fig. 5, physical ages estimated using the wind vector averaged from  
437 observed RAWS wind data are ~~75 minutes, 14, and 162 minutes~~ for April 6 (blue shading), 14 minutes for April 7  
438 (yellow shading) and 162 minutes for April 8 (green shading), 2021 events ~~respectively~~. For the same events and using  
439 HYSPLIT trajectories closest to the surface and passing through the identified sources, ages were estimated as 130  
440 minutes for April 6 (blue shading), 10 minutes for April 7 (yellow shading), and 40 minutes for April 8 (green  
441 shading) respectively. Based on our analysis, April 6 (blue shading) stands out as the only case where the HYSPLIT  
442 age exceeds that estimated using the mean wind vector for the same fire source. The difference between modeled and  
443 observed wind for these three instances was further investigated by comparison with the observed wind at Columbus  
444 Airport-substantial difference between modeled and observed winds suggests that relying on the wind vector based  
445 on observed winds is more reliable in this instance. As shown in Fig. S6, the wind direction observed at the airport  
446 aligns more closely with that observed at the RAWS site in Fort Moore (though with faster winds at the airport, likely  
447 due to the forest canopy effect on wind flow) than with the WRF modeled winds at both sites. However, it is difficult  
448 to determine which method is more reliable for studying any specific smoke event. For all the smoke plumes identified,  
449 the age of smoke estimated based on HYSPLIT back trajectories ranged from 10 minutes (single timestep of trajectory)  
450 to 6 hours (36 timesteps), and from a few minutes to 8 hours based on average wind vector method (Table S109). A  
451 comparison summary between wind speeds observed by the RAWS and those modeled by WRF during all the events

452 identified in 2021 and 2022 at the main trailer is shown in Fig. 6a. The observed weak correlation ( $r^2 = 0.29$ ) could be  
453 due to several factors. For the wind vector analysis, observed winds are measured at one location and 2 meters above  
454 ground level with a single monitor, which ~~may does~~ not accurately represent the wind patterns along the entire smoke  
455 transport path, especially in forested areas where the canopy can affect the attenuate wind flow (Mallia et al., 2020).  
456 On the other hand, WRF simulates winds for 34 layers at different altitudes from 10 m, being the lowest, to levels  
457 higher than the PBL. HYSPLIT applies bilinear interpolation to the data from WRF for the 10 trajectories that it  
458 calculates, introducing additional uncertainty to the wind patterns used in the simulations. Although the comparison  
459 between ages estimated based on the two different methods resulted in reasonable correlation ( $r^2=0.59$ ), the slope  
460 clearly indicates a significantly higher estimation of age when using the wind vector method, particularly for more  
461 aged smoke events, as shown in Fig. 6b, where ages from the two methods show stronger agreement for fresh smoke.  
462 This can be attributed, in many cases, to the uncertainty in observed winds during low-speed wind conditions, the  
463 measurement being far from where winds are observed (RAWS), and most importantly that RAWS measures winds  
464 at 2 m above ground level whereas smoke transport happens at higher altitudes with stronger winds. There are  
465 additional discrepancies resulting from wind variation at each altitude at which HYSPLIT is running.

#### 466 **2.6.3.5. Limitations of the fixed site method**

467 The goal of this project is to study the emissions and evolution of smoke from prescribed fires and provide  
468 data to test model simulations and assessments of prescribed burning impacts. Some limitations and challenges are  
469 associated with our approach of collecting data from a network of fixed sites.

#### 470 **3.5.1. Identification of burning regions**

471 First, due to the limitations of satellite fire detection, some fires were not seen in FIRMS satellite detection  
472 data but were subsequently identified from the fire management report, such as the prescribed fires on March 23,  
473 2021, shown in Fig. S76a. The 20-minute averaged  $PM_{2.5}$  mass concentration at the trailer increased to  $74.8 \mu g m^{-3}$ ,  
474 and to  $47.8 \mu g m^{-3}$  hourly average at the EPD site located off-base at the Columbus Airport in the afternoon of March  
475 23, 2021, as shown in the time series of Fig. S76b. This increase was accompanied by an elevation in the levels of  
476 CO,  $PM_{2.5}$  mass, BC, and BrC measured at the trailer. This is an example of burning on the Fort likely affecting the  
477 nearby urban population. Prevailing winds were from the southeast at the time of the smoke event, as can be seen from  
478 the wind vectors presented on the same time series in Fig. S76b. However, FIRMS satellite data showed no hotspots  
479 on the Fort during the entire day. After checking the fire management report for 2021, prescribed burns for 3 units  
480 located in the east central part of the Fort at distances ranging from 8.1 to 14.7 miles from the trailer were identified.  
481 Looking at either the wind vector at the time of the peak or the HYSPLIT back trajectories, the source of the smoke  
482 event identified on March 23, 2021 matches the closer prescribed burn conducted on the Fort.

483 Another issue with this approach is that relying only on data from the burning authorities at Fort Moore can,  
484 in some cases, be insufficient due to the lack of information about fires taking place off-base by landowners, such as  
485 the off-base fire seen on FIRMS during three overpasses of satellites at 12:38, 13:54, and 14:42 (Fig. S87a). On May  
486 9, 2022 at 16:30, monitored species increased at the main trailer and 20 minutes average of  $PM_{2.5}$  mass reached 52.3

487  $\mu\text{g m}^{-3}$  (Fig. S87b). The Fort's Fire Management reported no prescribed fires and one wildfire in the southern part of  
488 the base with an indication of zero probability of smoke from that fire reaching the trailer based on wind patterns.  
489 Based on both wind vectors and HYSPLIT simulations, the source of the event was identified as an off-base fire  
490 detected to the northeast of Fort Moore. The same smoke event was also observed at multiple trailers operating at the  
491 time and will be discussed more in the following section.

### 492 3.5.2. Identifying a specific fire impacting the site when multiple burning is occurring

493 When multiple fires are taking place simultaneously in varying wind conditions it can be difficult identifying  
494 the specific fire impacting the site, which can lead to uncertainty in the smoke age. This occurred in smoke detected  
495 around midnight on March 14, 2022 (see Fig. S98a). Relying on wind data, the smoke source is likely one or more of  
496 the fires on the east and/or southeast side of the base with a zero probability of it being one of the fires in the northern  
497 part of the base. HYSPLIT may help in narrowing down the possibilities of the smoke source (Fig. S98b), but there is  
498 still uncertainty in linking the specific fire to the observed event.

499 When several burning units are in close proximity and near the measurement site, identifying the specific  
500 source and smoke age can also be difficult (for example see Fig. S109). In this case burning in three units indicated  
501 by the Fort's Fire Management occurred at the same time close to each other and the trailer (distances of 0.6, 1.4, and  
502 2.2 miles from the trailer). HYSPLIT trajectory at lowest altitude passes near (to the east), but not over the prescribed  
503 fires. Wind direction at the time of the event suggests influence ~~from~~of a minor portion from the northern part of the  
504 fire. It is important to note that in such cases, transport near the surface may be heavily influenced by fire-atmosphere  
505 interactions, making it difficult to rely on data from RAWS or WRF simulations as accurate indicators of atmospheric  
506 flows close to an active fire.

507 We note that there is no direct correlation between the amount of smoke reaching the trailer, i.e., measured  
508 species concentrations, and the distance of the fire from the monitoring site. The relation depends on the smoke  
509 transport and dispersion that may allow smoke to either directly hit the measuring site, partially reach the measuring  
510 site, or pass above the trailer with little or no smoke detection by the monitors. To illustrate this, we compare three  
511 case studies. Looking again at the smoke event of February 11, 2022 shown in Fig. S109, smoke reaching the trailer  
512 from 0.6 to 2.2 miles fires resulted in a 20-minute maximum  $\text{PM}_{2.5}$  mass of  $62.8 \mu\text{g m}^{-3}$  and CO concentration of 1.3  
513 ppm at 13:30. On February 12, 2022 (Fig. S110 a and b), smoke from burns of units at distances 4.3 to 4.6 miles from  
514 the trailer, caused an increase in 20-minute  $\text{PM}_{2.5}$  mass concentration to  $60 \mu\text{g m}^{-3}$  and CO to 0.9 ppm at 13:50, whereas  
515 on the night of April 4, 2022 until the morning of April 5, 2022 (Fig. S110 c and d), smoke from fires 3.8 and 3.9  
516 miles from the trailer, caused an increase of 20-minute  $\text{PM}_{2.5}$  mass concentration to  $319 \mu\text{g m}^{-3}$  and CO to 3.0 ppm at  
517 1:10 over a longer smoke monitoring period. The much higher  $\text{PM}_{2.5}$  mass concentrations measured on April 4, 2022  
518 suggests that the trailer received a more direct smoke hit on that day than on February 11, 2022 or February 12, 2022,  
519 despite the fire being closer on February 11 and having a very similar distance to the one detected on February 12.  
520 This can also be attributed to the much lower nighttime PBL on April 4, which was 9.875 m and caused all HYSPLIT  
521 trajectories to overlap as shown in Fig. 12d. Emissions from a smoldering fire with very little buoyant energy were  
522 most likely trapped in this shallow layer leading to high concentration measurements. Higher PBL of 1645 and 1305



523 ~~m-d~~During the daytime on February 11 and 12, [higher PBL of 1645 and 1305 m](#), respectively, favored more vertical  
524 dispersion of smoke.

### 525 [3.5.3. Smoke not detected although regions of burning identified](#)

526 On certain days, based on the wind data and the information presented in the fire management report, it  
527 appears likely that smoke from the fires at the base should reach specific monitoring sites. However, during those  
528 instances, such as the situation on February 15, 2022 shown in Fig. 7, no significant smoke peaks were detected. To  
529 explain this outcome, two HYSPLIT forward trajectory simulations were run. The simulations show that if the fire  
530 starts at 10:00, the smoke will not intercept the monitor, but if it starts at 11:00, the smoke at higher altitudes has a  
531 slight chance of reaching the monitor. Overall, regardless of wind direction favoring smoke transport to monitors,  
532 other factors like dispersion and smoke plume behavior, such as lofting, play a significant role in the transport process.

### 533 ~~2.7.3.6. 3.6 Advantages of m~~[Using multiple monitoring sites to increase chances of measuring smoke and](#) 534 [studying smoke evolution](#)

535 There are distinct advantages of setting up multiple measuring sites and studying smoke over an extended  
536 period. First, it helps capture more smoke events, as seen during the 2022 study in comparison with that in 2021 when  
537 a single trailer was used. It minimizes issues with predicting downwind locations and is not affected by uncertainty in  
538 planned burning locations and times. Second, it reduces the labor and time required for relocating a single trailer and  
539 setting it up several times throughout a prescribed burning period where burning occurs over different regions. Third,  
540 it provides high spatial resolution and occasionally smoke from the same fire is detected at several sites, which can be  
541 useful in studying smoke chemical evolution with higher certainty than studies of multiple plumes of varying ages  
542 measured on different days.

543 ~~2.8.~~ An example of the same fire detected at several sites is shown in Fig. 8. On May 9, 2022, each of  
544 T1291, T1292, Main Trailer, and T1293 detected an off-base fire taking place approximately 11 miles to the north  
545 northeast of the base, as shown in Fig. 8a. T1291, the closest trailer to the fire, measured PM<sub>2.5</sub> mass and CO peaks at  
546 15:10. The time series of species measured in the various trailers is shown in Fig. 8. Subsequent peaks in PM<sub>2.5</sub> mass,  
547 CO, BC, and O<sub>3</sub> concentrations were recorded at T1292, at 15:50, then at the main trailer at 16:30, and finally at  
548 T1293, the furthest trailer from the fire, at 18:10 local time. For O<sub>3</sub>, note the O<sub>3</sub> enhancement ( $\Delta O_3$ ) superimposed on  
549 the diurnal O<sub>3</sub> trend. The ages of the smoke detected based on wind vector analysis were 266, 296, 330 and 480  
550 minutes, for the various trailers. [The difference in smoke age is close to the difference in peak arrival times with](#)  
551 [maximum PM<sub>2.5</sub> mass concentration observed at 15:02, 15:53, 16:25, and 18:16 on T1291, T1292, T1293, and T Main,](#)  
552 [respectively.](#) The differences in peak concentrations can be due to a number of factors, including changes in fire  
553 emissions with time, extent of plume dilution with distance from the fire and changes in what portions of the plume  
554 were measured due to changes in winds. Wind vectors are shown at the top of plots in Fig. 8. Wind direction and  
555 speed varied during the period when the plumes were recorded; wind direction was between 52° and 86° from 11:00  
556 till 14:00 and speeds between 3 and 7 mph on May 9, 2022. A shift in wind direction to 348° at a speed of 4 mph  
557 happened at 15:00. Then, the wind direction fluctuated between 11° and 44°, before wind speed decreased to 0 mph

558 at 20:00 and remained calm until the morning of May 10, 2022. Normalizing these plume data by a stable smoke  
559 tracer, such as CO, can account for some of these factors when comparing emissions and evolution of various plume  
560 properties.

### 561 [3.7. 3.7 Interpretation of measurements to characterize smoke emissions and evolution](#)

#### 562 [3.7.1 PM<sub>2.5</sub> emissions](#)

563 We used the normalized excess mixing ratio (NEMR) to study the emissions of PM<sub>2.5</sub> species and their  
564 evolution in the various measured smoke plumes. The NEMRs determined from the linear regression slopes of PM<sub>2.5</sub>  
565 species (mass concentration, BC concentration, BrC absorption versus CO, with backgrounds subtracted) and  
566 correlation values ( $r^2$ ) for all smoke events are summarized in Table 1. PM<sub>2.5</sub> mass concentration NEMRs from other  
567 studies are summarized in Table S119.

568 The NEMR of fresh smoke near a fire is interpreted as an emission ratio (ER), assuming the smoke has  
569 undergone limited chemical and/or physical changes. ERs based on NEMRs are widely used (Liu et al., 2017b; Collier  
570 et al., 2016; Burling et al., 2011; Gkatzelis et al., 2024). They are compiled in reviews and emission inventories for  
571 ambient (Andreae, 2019; Prichard et al., 2020) and laboratory fire studies (Yokelson et al., 2013), and for evaluating  
572 or making model predictions (Xiu et al., 2022; Jaffe et al., 2022).

573 By focusing on fresh smoke (age less than 1 hour), the emissions ratios (ER) of the prescribed fires can be  
574 estimated and compared to those from other studies. The PM<sub>2.5</sub> mass concentration ER ranged between 0.04 and 0.18  
575  $\mu\text{g m}^{-3} \text{ppb}^{-1}$  and is shown in Fig. 9. These ERs are comparable to other prescribed fires measured at both ground level  
576 (Alves et al., 2010; Desservettaz et al., 2017; Korontzi et al., 2003; Balachandran et al., 2013) and aloft in airborne  
577 studies (Sinha et al., 2003; May et al., 2014; Gkatzelis et al., 2024; Travis et al., 2023) that span a large range of  
578 burning conditions and fuels (details are provided in Table S119). The mean PM<sub>2.5</sub> mass concentration ER for our data  
579 is  $0.117 \pm 0.045 \mu\text{g m}^{-3} \text{ppb}^{-1}$  and that of these other prescribed fire studies are  $0.098 \pm 0.034 \mu\text{g m}^{-3} \text{ppb}^{-1}$  for ground-  
580 based and  $0.18845 \pm 0.154086 \mu\text{g m}^{-3} \text{ppb}^{-1}$  for airborne measurements. There is substantial and similar variability in  
581 the ground-based measurements of prescribed fire ERs in this study relative to other studies. ~~However, some~~ More  
582 recent airborne-measured prescribed fires have reported substantially higher ERs (Fig. 9). Smoke transported for 10  
583 minutes from the Blackwater river state forest prescribed fire reported by Gkatzelis et al. had an ER of  $0.462 \mu\text{g m}^{-3}$   
584  $\text{ppb}^{-1}$  (Gkatzelis et al., 2024) and Travis et al. reported a range of 0.188-0.433  $\mu\text{g m}^{-3} \text{ppb}^{-1}$  for 22 prescribed fires  
585 studied and grouped into 4 categories based on fuel type (Travis et al., 2023) ~~Burling et al. reported an ER of 0.399~~  
586  ~~$\mu\text{g m}^{-3} \text{ppb}^{-1}$  for the Bear Pen prescribed fire in NC (Burling et al., 2011)~~. Figure 9 also shows comparisons with  
587 wildfires reported in other studies (Liu et al., 2017b; Collier et al., 2016; Palm et al., 2020; Gkatzelis et al., 2024).  
588 Wildfire PM<sub>2.5</sub> mass ERs are significantly higher than ERs for prescribed fires in this work, with ER ranges between  
589 0.04 and  $0.43 \mu\text{g m}^{-3} \text{ppb}^{-1}$  and a mean of  $0.264 \pm 0.091 \mu\text{g m}^{-3} \text{ppb}^{-1}$  for wildfires, and the difference is statistically  
590 significant (two-tailed p value is  $< 0.0001$ ). Lower PM<sub>2.5</sub> mass ERs from smaller prescribed fires has been noted in  
591 other studies (Liu et al., 2017b) and supports utilizing prescribed burning as a land management tool to limit wildfires.  
592 However, differences in altitude at which the measurements were made may have some effect on ERs. Selimovic et  
593 al. (Selimovic et al., 2019) noted that the PM<sub>2.5</sub>/CO in ground-level smoke was about half of that observed from aloft

594 apparently due to reduction in aerosol mass from evaporation of semi-volatile aerosol particle components resulting  
595 from higher surface temperatures compared to aloft. Pagonis et al. also found airborne OA NEMRs to be a factor of 2  
596 higher than ground-based NEMRs giving the same interpretation (Pagonis et al., 2023). However, wWhen comparing  
597 ERs of prescribed fires in ground versus airborne studies of prescribed fires, shown in Fig. 9, the mean of airborne  
598 studies is a factor of ~ 1.9 higher than ground-based studies and the difference is statistically significant (p value is  
599 0.025).difference is not significant (p value is 0.435).

600 This analysis assumes no significant changes in PM<sub>2.5</sub> mass for smoke less than 1 hour old. We have seen  
601 that smoke detected in the afternoon can have enhanced O<sub>3</sub> concentrations, which may also lead to secondary aerosol  
602 formation. Smoke plumes with enhanced O<sub>3</sub> are identified in the ERs shown in Fig. 9 and indicate no bias within the  
603 range of ERs recorded, suggesting possible secondary aerosol formation within the first hour following emissions  
604 does not contribute to the ER variability. We also did not find evidence of ERs depending on time of day. No difference  
605 was seen between ERs for fires that started on the same day of measurement (i.e., all detected after 9:00 and before  
606 17:00), and those detected at night, after 17:00, or early in the morning corresponding to fires that started the day  
607 before the measurement, but still were estimated to correspond to smoke less than one hour old.

608 We also determined the ERs for BC and BrC. BC ERs were in the range of 0.008–0.022 μg m<sup>-3</sup> ppb<sup>-1</sup> with a  
609 mean value of 0.014 ± 0.004 μg m<sup>-3</sup> ppb<sup>-1</sup>, which are within the range of NEMRs reported in other studies; 0.006 μg  
610 m<sup>-3</sup> ppb<sup>-1</sup> for prescribed burns in southern African savanna forests (Sinha et al., 2003), 0.020 μg m<sup>-3</sup> ppb<sup>-1</sup> for rBC  
611 (refractory BC) for prescribed burns of California chaparral forests (Akagi et al., 2012), 0.022 μg m<sup>-3</sup> ppb<sup>-1</sup> for  
612 chaparral forests (May et al., 2014), 0.006 μg m<sup>-3</sup> ppb<sup>-1</sup> for fires in Montane ecosystems (May et al., 2014), 0.018 for  
613 coastal plain ecosystems in South Carolina (May et al., 2014), and 0.004 μg m<sup>-3</sup> ppb<sup>-1</sup> for large wildfires over the  
614 western US measured during FIREX (Gkatzelis et al., 2024).

615 The BrC ERs of fresh smoke events ranged between 0.151 and 0.689 Mm<sup>-1</sup> ppb<sup>-1</sup> with a mean ± standard  
616 deviation of 0.442 ± 0.157 Mm<sup>-1</sup> ppb<sup>-1</sup>. There is limited published data on BrC ERs and NEMRs from prescribed fires  
617 and the measurement techniques of BrC vary between studies. Liu et al. (Liu et al., 2016) reported aircraft  
618 measurements of BrC at 365 nm inferred from PSAP absorption coefficients measured at two wavelengths (470 and  
619 532 nm) with an ER of 0.223 ± 0.053 Mm<sup>-1</sup> ppb<sup>-1</sup> for fresh agricultural fires in the southeastern US, which is lower  
620 than our mean, but falls within the range of values we observed. For large wildfires measured over the western US,  
621 Zeng et al. (Zeng et al., 2022) found for Photoacoustic Spectroscopy (PAS) measurements of BrC at a wavelength of  
622 405 nm, the ER was 0.131 ± 0.001 Mm<sup>-1</sup> ppbv<sup>-1</sup> in plumes < 2 hours old. These values are in the range we recorded,  
623 but the BrC ERs for the prescribed fires of this study are more variable.

### 624 ***3.8-7.2 NEMRs of all smoke events and their change with smoke age***

625 Here we assess the overall variability in NEMRs for PM<sub>2.5</sub> mass concentrations, BC mass concentrations,  
626 BrC absorption coefficients, and AAEs from all the smoke events (including ages less than 1 hour) and assess possible  
627 trends with smoke plume age. In this analysis, the observed changes with age are a combination of variability in  
628 emissions and evolution of the aerosol since it is not a Lagrangian experiment, meaning that we are not continuously

629 tracking a specific air mass containing smoke particles over time. PM<sub>2.5</sub> mass concentration NEMRs varied between  
630 0.04 and 0.47 μg m<sup>-3</sup> ppb<sup>-1</sup> for all reported events with a mean ± standard deviation of 0.155 ± 0.076 μg m<sup>-3</sup> ppb<sup>-1</sup>  
631 (median is 0.138 μg m<sup>-3</sup> ppb<sup>-1</sup>). BC NEMRs ranged between 0.005 and 0.024 μg m<sup>-3</sup> ppb<sup>-1</sup> with a mean value of 0.013  
632 ± 0.005 μg m<sup>-3</sup> ppb<sup>-1</sup>. BrC NEMRs (ΔBrC/ΔCO) varied between 0.133 to 1.550 Mm<sup>-1</sup> ppb<sup>-1</sup>. (Note that data collected  
633 on April 21, 2022 at trailer 1293 is an outlier with exceptionally high ERs for PM<sub>2.5</sub> mass concentration and BrC  
634 absorption coefficient. The ER for BC mass concentration, while elevated, falls within the observed range. This event  
635 corresponds to smoke from an identified prescribed fire at the Fort and has a relatively low ΔCO of 66.1 ppb, which  
636 is unexpected given the burn's proximity and the wind ~~speed~~ conditions on that day, causing ERs to be significantly  
637 higher. The HYSPLIT back trajectory from the measuring site does not intersect with the fire but passes close to it.  
638 Although the FRP reported on FIRMS does not differ from that of other fires, and there is no significant difference in  
639 vegetation type or fuel moisture, the most likely explanation for this event is that the smoke passing through the  
640 measurement site was not a direct hit but from the diluted boundary of the plume, which may have undergone  
641 photochemical processing, leading to higher PM<sub>2.5</sub>, BrC, and O<sub>3</sub> NEMRs.) The NEMRs are given in Table 1 for all  
642 smoke events data and plotted in Fig. 10 as a function of estimated smoke age determined from the wind vector and  
643 HYSPLIT analysis. From these plots we assess if there is any systematic evolution of the PM<sub>2.5</sub> mass, BC and BrC.

644 ***Changes in PM<sub>2.5</sub> Mass Concentration NEMR with smoke age:*** From Fig. 10a, PM<sub>2.5</sub> mass concentration  
645 NEMR shows substantial variability at all ages with no significant statistical difference or clear trend, however, NEMR  
646 tends to be lower for fresh smoke events (≤ 1 hour old) versus more aged plumes, possibly from secondary aerosol  
647 formation. Considering only smoke plumes in which O<sub>3</sub> enhancements were observed (i.e., smoke measured between  
648 12:00 and 18:00), PM<sub>2.5</sub> mass concentration NEMR consistently increases with physical age (r<sup>2</sup>=\_0.65), possibly  
649 evidence of secondary aerosol formation driven by photochemistry through a photochemical process that directly  
650 involve O<sub>3</sub>, or some other related oxidant, (e.g., OH) (Liu et al., 2016).

651 A range of results for changes in PM<sub>2.5</sub> mass concentration NEMRs in wildland fires have been observed in  
652 other studies, including systematic increases, little change, or decreases with smoke age. To the best of our knowledge,  
653 no ground-based studies have been conducted on the evolution of smoke from prescribed fires, but frequent airborne  
654 studies have investigated prescribed and wildland smoke aging because of the ability to spatially characterize a single  
655 plume. While studying two prescribed fires in SC, May et al. (May et al., 2015) observed no statistically significant  
656 net change in OA NEMRs near the source and downwind for smoke transported for ≤ 1.5 hours. One of the two fires  
657 was studied for longer, and results showed downwind OA NEMRs over 2 to 5 hours of transport significantly lower  
658 than the NEMRs at the source, suggesting a net loss of emitted OA. ~~Also, a decrease in OA/CO from 0.057 to 0.046~~  
659 ~~μg m<sup>-3</sup> ppb<sup>-1</sup> was reported after 4 hours in an airborne study of an 81 hectare prescribed fire in chaparral fuels on the~~  
660 ~~central coast of California (Akagi et al., 2012). In contrast, an airborne study of 20 deforestation and crop residue fires~~  
661 ~~on the Yucatan peninsula, reported an increase in PM<sub>2.5</sub> NEMRs by a factor of 2.6 (NEMR increased from 0.072 to~~  
662 ~~0.187 μg m<sup>-3</sup> ppb<sup>-1</sup>) in the first 1.4 hours due to rapid secondary formation of organic and inorganic aerosol (Yokelson~~  
663 ~~et al., 2009).~~ For wildfires, Collier et al. (Collier et al., 2016) found increases, little change, and decreases with smoke  
664 age in different wildfire plumes measured in Oregon. For the selected large wildfires in the western US in summer,

665 Palm et al. (Palm et al., 2020) reported that the OA NEMR remained almost constant at a value of  $\sim 0.25 \mu\text{g m}^{-3} \text{ppb}^{-1}$   
666 <sup>1</sup> as the plume aged from 20-50 minutes to 6 hours. In their analysis of the data of wildland fires studied during FIREX-  
667 AQ campaign in 2019, Pagonis et al. report OA NEMR increased from  $0.2 \text{ g g}^{-1}$  to  $0.3 \text{ g g}^{-1}$  in 3 hours (Pagonis et al.,  
668 2023). While Garofalo et al. found no significant change of NEMRs between 0.5-8 hours transport of smoke from 20  
669 western wildfires, they concluded that there was secondary OA formation through oxidation driven condensation, but  
670 it was balanced by dilution-driven evaporation (Garofalo et al., 2019). Gkatzelis et al. reported the NEMRs of some  
671 plumes that were more than an hour old and are shown in Table S101 with their corresponding physical age (Gkatzelis  
672 et al., 2024). For the same fire (William's flat), the NEMR was  $0.331 \mu\text{g m}^{-3} \text{ppb}^{-1}$  at a physical age of 15 minutes that  
673 increased to  $0.524 \mu\text{g m}^{-3} \text{ppb}^{-1}$  at 102 minutes (Gkatzelis et al., 2024). Similar increase for the Castle fire was seen  
674 where the NEMRs reported are 0.204, 0.244, and  $0.463 \mu\text{g m}^{-3} \text{ppb}^{-1}$  at 25, 27, and 153 minutes respectively. For  
675 another fire (Horsefly), the NEMR was  $0.398 \mu\text{g m}^{-3} \text{ppb}^{-1}$  at a physical age of 65 minutes and remained at a similar  
676 value of  $0.391 \mu\text{g m}^{-3} \text{ppb}^{-1}$  at 104 minutes. On average, the mean NEMRs for plumes of physical age less than one  
677 hour, reported in their study, was  $0.218 \pm 0.110$ . This value is lower than that of plumes older than one hour, which  
678 have a mean value of  $0.391 \pm 0.131$  (Gkatzelis et al., 2024). Overall, we find no trends in our data when considering  
679 all the smoke plumes detected, but for periods of expected photochemical activity we observe consistent evidence for  
680 aerosol formation with plume age, which might be attributed to the optically thin smoke that allows photochemistry  
681 throughout the plume compared to large optically thick wildfires that leads to more complex photochemistry within  
682 the plume (Decker et al., 2021a).

683 We examined other factors that may contribute to variability of  $\text{PM}_{2.5}$  mass NEMRs. No significant difference  
684 was observed between on-base and off-base sources of smoke. Mean  $\text{PM}_{2.5}$  mass NEMR of smoke originating from  
685 outside the base is 0.208 (range  $0.112\text{--}0.277 \mu\text{g m}^{-3} \text{ppb}^{-1}$ ), compared to  $0.147 \mu\text{g m}^{-3} \text{ppb}^{-1}$  (range  $0.042\text{--}0.466 \mu\text{g}$   
686  $\text{m}^{-3} \text{ppb}^{-1}$ ) for on base burning, which is not statistically different (two tailed p-value is 0.076). A preliminary  
687 assessment using Google Earth Satellite imagery and Landscape Fire and Resources Management Planning Tool  
688 (LANDFIRE, <https://www.landfire.gov/>) does not show any visible differences in vegetation between the forested  
689 areas burnt on and off the base. Additionally, no further information regarding the fuel types in the off-base lands  
690 could be obtained. Just like no detected differences being observed between day/night  $\text{PM}_{2.5}$  mass concentration ERs,  
691 there was no significant difference (p-value is 0.169) between smoke plumes of all ages measured during the day  
692 corresponding to fires occurring within a few hours from starting the burn (after 9:00 and before 17:00) (mean NEMR  
693 =  $0.178 \mu\text{g m}^{-3} \text{ppb}^{-1}$ ) and those monitored at night and early in the morning corresponding to fires starting the day  
694 before (after 17:00) (mean NEMR =  $0.137 \mu\text{g m}^{-3} \text{ppb}^{-1}$ ), in contrast to an observed trend of  $\text{PM}_{2.5}$  mass NEMR with  
695 age for smoke with  $\text{O}_3$  enhancement. This may suggest little night-time secondary aerosol formation- (Brown et al.,  
696 2013), but a more focused analysis is needed to better assess possible evidence for secondary aerosol formation. No  
697 correlation was observed between  $\text{PM}_{2.5}$  mass NEMRs and relative humidity ( $r^2 = 0.08$ ) or fuel moisture data ( $r^2 =$   
698  $0.04$ ) for the smoke events in this study (Fig. S132). A weak positive correlation between air temperature and  $\text{PM}_{2.5}$   
699 mass NEMRs was observed, with an  $r^2$  of 0.14 for all smoke events and  $r^2$  of 0.44 for fresh smoke events. Many factors  
700 could cause variability in  $\text{PM}_{2.5}$  mass NEMRs, but no single factor could be identified when all data from this study  
701 is grouped together.

702 *Changes in BC and BrC NEMR with smoke age:* BC and BrC NEMRs versus age are shown in Fig. 10b  
703 and 10c with periods of O<sub>3</sub> enhancements identified. No trend in BC NEMRs with age is observed, as expected, since  
704 BC is primarily emitted and largely nonvolatile. Lack of a trend supports this analysis approach, and all the BC  
705 measured in events largely reflects BC variability in emissions relative to CO. BrC NEMRs are also highly variable  
706 and have no trend with age for all the data or just the periods of O<sub>3</sub> enhancements. Since BrC can be both primary and  
707 secondary, is semi-volatile, and undergoes photo-bleaching, a range of results on BrC evolution has been observed in  
708 past studies (Zhong and Jang, 2014; Saleh et al., 2013; Liu et al., 2016). Like BC, a similar large variability, with no  
709 trend, in BrC NEMRs with ages up to 8 hours has been observed for wildfires in the western US (Zeng et al., 2022;  
710 Sullivan et al., 2022; Palm et al., 2020) whereas in some cases consistent loss (bleaching) of BrC has been reported  
711 (Forrister et al., 2015). Optical properties of absorptive aerosol spectral properties characterized by AAE are shown  
712 in Fig. 11 as a function of age. Total absorption AAE values from the two trailers with 7-wavelength aethalometers  
713 (i.e., BC+BrC measured by the aethalometer) varied between 1.31 and 3.32 (mean  $\pm$  stdev of  $1.89 \pm 0.23$ ) and between  
714 3.19 and 7.43 (mean =  $5.00 \pm 0.89$ ) for BrC only. AAEs have no trend with age for either fresh smoke plumes or  
715 periods of O<sub>3</sub> enhancement. While our total AAE values are similar (Zeng et al., 2022; Strand et al., 2016; Marsavin  
716 et al., 2023) or sometimes lower (Liu et al., 2016; Forrister et al., 2015) than those in other biomass burning studies,  
717 it is indicative of the presence of BrC in the smoke plumes studied. As for BrC AAEs, our reported values are  
718 significantly higher than those reported for western wildfires, where BrC determined from the PAS had an AAE of  
719  $2.07 \pm 1.01$  (Zeng et al., 2022), indicating difference in BrC optical properties or with instrumentation, which needs  
720 further investigation. Selimovic et al. show that duff has the highest AAE of 7.13 (calculated from absorption data at  
721 401 and 870 nm) when burnt, and it is typically consumed more in wildfires than in prescribed fires. However, the  
722 variability in optical properties is influenced more by the differential consumption of individual components than by  
723 the dominant tree species in the ecosystem (Selimovic et al., 2019).

#### 724 **3.4. Conclusion**

725 We describe a ground-based observational study measurement method for characterizing smoke from  
726 prescribed fires based on continuous monitoring at multiple sites for an extended period in a regularly burned region.  
727 We focus on burning within a large military Fort in the southeastern US and identify the sources of the smoke to  
728 determine if it was within or outside the Fort and study emissions and evolution of smoke species. The method was  
729 successful in capturing a significant number of smoke events (64) monitored on 42 days and linked to 45 fires across  
730 2 burning seasons. Source and age for each smoke plume detected was estimated~~determined~~. This allowed us to match  
731 95 % of the identified events to their corresponding source and to calculate the estimated transport time of smoke from  
732 source to monitors. These data were used to characterize emissions and evolution of key smoke parameters through  
733 calculation of normalized excess mixing ratios (NEMRs), with CO as the conserved co-emitted species~~ative~~  
734 parameter. Overall, PM<sub>2.5</sub> mass concentration NEMRs ( $\Delta$ PM<sub>2.5</sub> mass/ $\Delta$ CO) ranged between 0.04 and 0.47  $\mu\text{g m}^{-3} \text{ppb}^{-1}$   
735 <sup>1</sup> with a study mean of  $0.155 \pm 0.076 \mu\text{g m}^{-3} \text{ppb}^{-1}$  (median is  $0.138 \mu\text{g m}^{-3} \text{ppb}^{-1}$ ). For plumes less than 1 hour old the  
736 PM<sub>2.5</sub> mass concentration NEMRs were interpreted as a characteristic of the fire's emissions. Emissions ratios for fires  
737 of this study ranged between 0.042 and 0.176  $\mu\text{g m}^{-3} \text{ppb}^{-1}$  with a mean of  $0.117 \pm 0.045 \mu\text{g m}^{-3} \text{ppb}^{-1}$  (median is 0.121

738  $\mu\text{g m}^{-3}$  ppb<sup>-1</sup>). These emissions estimates are in the range reported in other ground-based studies for a range of fires  
739 and fuels but are lower than what has been reported for wildfire smoke measured from aircraft at higher altitudes. BC  
740 and BrC NEMRs and emission ratios are also reported. An analysis of PM<sub>2.5</sub> mass and BrC NEMRs changes with  
741 smoke age showed no consistent trends for all combined smoke plumes. However, PM<sub>2.5</sub> mass NEMRs did increase  
742 with age for smoke detected in the afternoon in plumes where O<sub>3</sub> enhancements were observed, indicating ~~the~~  
743 ~~combined secondary O<sub>3</sub> and particle mass~~ formation of O<sub>3</sub> and secondary organic aerosol. This was not observed for  
744 BrC NEMRs. This data set will be used to assess models predicting the impact of prescribed fires on air quality to  
745 enhance the use of prescribed burning in land management practices by minimizing impacts on populations.  
746

#### 747 **4.5. Competing interests**

748 The contact author has declared that none of the authors has any competing interests.  
749

#### 750 **5.6. Acknowledgements**

751 We thank Fort Moore authorities for hosting the field study, and to the members of the Natural Resources Management  
752 Branch for sharing information about the burns. REA, DJT, GH and RJW were supported by the United States Army  
753 Corps of Engineers under contract W912HQ-20-C-0019. ZL, YH, and MTO were supported by the Strategic  
754 Environmental Research and Development Program (SERDP) through project RC20-1047.  
755

756 **Author contribution:** REA and RJW wrote the paper. RJW, LGH, DJT, and MTO designed the experiment. REA  
757 and DJT collected the data. REA, ZL, DJT, and RJW analyzed data. REA and ZL worked on the HYSPLIT analysis.  
758 All authors reviewed and provided comments for the paper.

759

760 **Data availability:** Data are available in a publicly accessible repository: <https://doi.org/10.5281/zenodo.11222295>.

761 **References**

- 762 Afrin, S. and Garcia-Menendez, F.: The Influence of Prescribed Fire on Fine Particulate Matter Pollution in the  
763 Southeastern United States, *Geophys. Res. Lett.*, 47, <https://doi.org/10.1029/2020GL088988>, 2020.
- 764 Akagi, S. K., Craven, J. S., Taylor, J. W., McMeeking, G. R., Yokelson, R. J., Burling, I. R., Urbanski, S. P., Wold,  
765 C. E., Seinfeld, J. H., Coe, H., Alvarado, M. J., and Weise, D. R.: Evolution of trace gases and particles emitted by a  
766 chaparral fire in California, *Atmos. Chem. Phys.*, 12, 1397–1421, <https://doi.org/10.5194/acp-12-1397-2012>, 2012.
- 767 Akagi, S. K., Burling, I. R., Mendoza, A., Johnson, T. J., Cameron, M., Griffith, D. W. T., Paton-Walsh, C., Weise,  
768 D. R., Reardon, J., and Yokelson, R. J.: Field measurements of trace gases emitted by prescribed fires in  
769 southeastern US pine forests using an open-path FTIR system, *Atmos. Chem. Phys.*, [https://doi.org/10.5194/acp-14-](https://doi.org/10.5194/acp-14-199-2014)  
770 199-2014, 2014.
- 771 Alves, C. A., Gonçalves, C., Pio, C. A., Mirante, F., Caseiro, A., Tarelho, L., Freitas, M. C., and Viegas, D. X.:  
772 Smoke emissions from biomass burning in a Mediterranean shrubland, *Atmos. Environ.*, 44, 3024–3033,  
773 <https://doi.org/10.1016/j.atmosenv.2010.05.010>, 2010.
- 774 Andreae, M. O.: Emission of trace gases and aerosols from biomass burning – an updated assessment, *Atmos.*  
775 *Chem. Phys.*, 19, 8523–8546, <https://doi.org/10.5194/acp-19-8523-2019>, 2019.
- 776 Aurell, J. and Gullett, B. K.: Effects of UAS Rotor Wash on Air Quality Measurements, *Drones*, 8, 73,  
777 <https://doi.org/10.3390/drones8030073>, 2024.
- 778 Aurell, J., Gullett, B., Holder, A., Kiros, F., Mitchell, W., Watts, A., and Ottmar, R.: Wildland fire emission  
779 sampling at Fishlake National Forest, Utah using an unmanned aircraft system, *Atmos. Environ.*, 247, 118193,  
780 <https://doi.org/10.1016/j.atmosenv.2021.118193>, 2021.
- 781 Balachandran, S., Pachon, J. E., Lee, S., Oakes, M. M., Rastogi, N., Shi, W., Tagaris, E., Yan, B., Davis, A., Zhang,  
782 X., Weber, R. J., Mulholland, J. A., Bergin, M. H., Zheng, M., and Russell, A. G.: Particulate and gas sampling of  
783 prescribed fires in South Georgia, USA, *Atmos. Environ.*, 81, 125–135,  
784 <https://doi.org/10.1016/j.atmosenv.2013.08.014>, 2013.
- 785 Bell, M. L.: Ozone and Short-term Mortality in 95 US Urban Communities, 1987-2000, *JAMA*, 292, 2372,  
786 <https://doi.org/10.1001/jama.292.19.2372>, 2004.
- 787 Bond, T. C., Anderson, T. L., and Campbell, D.: Calibration and Intercomparison of Filter-Based Measurements of  
788 Visible Light Absorption by Aerosols, *Aerosol Sci. Technol.*, <https://doi.org/10.1080/027868299304435>, 1999.
- 789 Borchers-Arriagada, N., Bowman, D. M. J. S., Price, O., Palmer, A. J., Samson, S., Clarke, H., Sepulveda, G., and  
790 Johnston, F. H.: Smoke health costs and the calculus for wildfires fuel management: a modelling study, *Lancet*  
791 *Planet. Heal.*, [https://doi.org/10.1016/S2542-5196\(21\)00198-4](https://doi.org/10.1016/S2542-5196(21)00198-4), 2021.
- 792 Brown, S. S., Dubé, W. P., Bahreini, R., Middlebrook, A. M., Brock, C. A., Warneke, C., de Gouw, J. A.,



793 Washenfelder, R. A., Atlas, E., Peischl, J., Ryerson, T. B., Holloway, J. S., Schwarz, J. P., Spackman, R., Trainer,  
794 M., Parrish, D. D., Fehshenfeld, F. C., and Ravishankara, A. R.: Biogenic VOC oxidation and organic aerosol  
795 formation in an urban nocturnal boundary layer: aircraft vertical profiles in Houston, TX, *Atmos. Chem. Phys.*, 13,  
796 11317–11337, <https://doi.org/10.5194/acp-13-11317-2013>, 2013.

797 Burling, I. R., Yokelson, R. J., Akagi, S. K., Urbanski, S. P., Wold, C. E., Griffith, D. W. T., Johnson, T. J.,  
798 Reardon, J., and Weise, D. R.: Airborne and ground-based measurements of the trace gases and particles emitted by  
799 prescribed fires in the United States, *Atmos. Chem. Phys.*, 11, 12197–12216, [https://doi.org/10.5194/acp-11-12197-](https://doi.org/10.5194/acp-11-12197-2011)  
800 2011, 2011.

801 Christopher, S. A., Chou, J., Welch, R. M., Kliche, D. V., and Connors, V. S.: Satellite investigations of fire, smoke,  
802 and Carbon Monoxide during April 1994 MAPS mission: Case studies over tropical Asia, *J. Geophys. Res. Atmos.*,  
803 <https://doi.org/10.1029/97JD01813>, 1998.

804 Collier, S., Zhou, S., Onasch, T. B., Jaffe, D. A., Kleinman, L., Sedlacek, A. J., Briggs, N. L., Hee, J., Fortner, E.,  
805 Shilling, J. E., Worsnop, D., Yokelson, R. J., Parworth, C., Ge, X., Xu, J., Butterfield, Z., Chand, D., Dubey, M. K.,  
806 Pekour, M. S., Springston, S., and Zhang, Q.: Regional Influence of Aerosol Emissions from Wildfires Driven by  
807 Combustion Efficiency: Insights from the BBOP Campaign, *Environ. Sci. Technol.*, 50, 8613–8622,  
808 <https://doi.org/10.1021/acs.est.6b01617>, 2016.

809 Cubison, M. J., Ortega, A. M., Hayes, P. L., Farmer, D. K., Day, D., Lechner, M. J., Brune, W. H., Apel, E., Diskin,  
810 G. S., Fisher, J. A., Fuelberg, H. E., Hecobian, A., Knapp, D. J., Mikoviny, T., Riemer, D., Sachse, G. W., Sessions,  
811 W., Weber, R. J., Weinheimer, A. J., Wisthaler, A., and Jimenez, J. L.: Effects of aging on organic aerosol from  
812 open biomass burning smoke in aircraft and laboratory studies, *Atmos. Chem. Phys.*, [https://doi.org/10.5194/acp-11-](https://doi.org/10.5194/acp-11-12049-2011)  
813 12049-2011, 2011.

814 Decker, Z. C. J., Robinson, M. A., Barsanti, K. C., Bourgeois, I., Coggon, M. M., DiGangi, J. P., Diskin, G. S.,  
815 Flocke, F. M., Franchin, A., Fredrickson, C. D., Gkatzelis, G. I., Hall, S. R., Halliday, H., Holmes, C. D., Huey, L.  
816 G., Lee, Y. R., Lindaas, J., Middlebrook, A. M., Montzka, D. D., Moore, R., Neuman, J. A., Nowak, J. B., Palm, B.  
817 B., Peischl, J., Piel, F., Rickly, P. S., Rollins, A. W., Ryerson, T. B., Schwantes, R. H., Sekimoto, K., Thornhill, L.,  
818 Thornton, J. A., Tyndall, G. S., Ullmann, K., Van Rooy, P., Veres, P. R., Warneke, C., Washenfelder, R. A.,  
819 Weinheimer, A. J., Wiggins, E., Winstead, E., Wisthaler, A., Womack, C., and Brown, S. S.: Nighttime and daytime  
820 dark oxidation chemistry in wildfire plumes: an observation and model analysis of FIREX-AQ aircraft data, *Atmos.*  
821 *Chem. Phys.*, 21, 16293–16317, <https://doi.org/10.5194/acp-21-16293-2021>, 2021a.

822 Decker, Z. C. J., Wang, S., Bourgeois, I., Campuzano Jost, P., Coggon, M. M., DiGangi, J. P., Diskin, G. S., Flocke,  
823 F. M., Franchin, A., Fredrickson, C. D., Gkatzelis, G. I., Hall, S. R., Halliday, H., Hayden, K., Holmes, C. D., Huey,  
824 L. G., Jimenez, J. L., Lee, Y. R., Lindaas, J., Middlebrook, A. M., Montzka, D. D., Neuman, J. A., Nowak, J. B.,  
825 Pagonis, D., Palm, B. B., Peischl, J., Piel, F., Rickly, P. S., Robinson, M. A., Rollins, A. W., Ryerson, T. B.,  
826 Sekimoto, K., Thornton, J. A., Tyndall, G. S., Ullmann, K., Veres, P. R., Warneke, C., Washenfelder, R. A.,  
827 Weinheimer, A. J., Wisthaler, A., Womack, C., and Brown, S. S.: Novel Analysis to Quantify Plume Crosswind

828 Heterogeneity Applied to Biomass Burning Smoke, *Environ. Sci. Technol.*, <https://doi.org/10.1021/acs.est.1c03803>,  
829 2021b.

830 Deng, A., Stauffer, D., Guadet, B., Dudhia, J., Hacker, J., Bruyere, C., Wu, W., Vandenberghe, F., Liu, Y., and  
831 Bourgeois, A.: A. 1.9 Update on WRF-ARW End-to-End Multi-Scale FDDA System, in: In Proceedings of the  
832 WRF Users' Workshop, 2009.

833 Desservettaz, M., Paton-Walsh, C., Griffith, D. W. T., Kettlewell, G., Keywood, M. D., Vanderschoot, M. V., Ward,  
834 J., Mallet, M. D., Milic, A., Miljevic, B., Ristovski, Z. D., Howard, D., Edwards, G. C., and Atkinson, B.: Emission  
835 factors of trace gases and particles from tropical savanna fires in Australia, *J. Geophys. Res. Atmos.*, 122, 6059–  
836 6074, <https://doi.org/10.1002/2016JD025925>, 2017.

837 Fiddler, M. N., Thompson, C., Pokhrel, R. P., Majluf, F., Canagaratna, M., Fortner, E. C., Daube, C., Roscioli, J. R.,  
838 Yacovitch, T. I., Herndon, S. C., and Bililign, S.: Emission Factors From Wildfires in the Western US: An  
839 Investigation of Burning State, Ground Versus Air, and Diurnal Dependencies During the FIREX-AQ 2019  
840 Campaign, *J. Geophys. Res. Atmos.*, 129, <https://doi.org/10.1029/2022JD038460>, 2024.

841 Fleming, L. T., Lin, P., Roberts, J. M., Selimovic, V., Yokelson, R., Laskin, J., Laskin, A., and Nizkorodov, S. A.:  
842 Molecular composition and photochemical lifetimes of brown carbon chromophores in biomass burning organic  
843 aerosol, *Atmos. Chem. Phys.*, 20, 1105–1129, <https://doi.org/10.5194/acp-20-1105-2020>, 2020.

844 Forrister, H., Liu, J., Scheuer, E., Dibb, J., Ziemba, L., Thornhill, K. L., Anderson, B., Diskin, G., Perring, A. E.,  
845 Schwarz, J. P., Campuzano-Jost, P., Day, D. A., Palm, B. B., Jimenez, J. L., Nenes, A., and Weber, R. J.: Evolution  
846 of brown carbon in wildfire plumes, *Geophys. Res. Lett.*, 42, 4623–4630, <https://doi.org/10.1002/2015GL063897>,  
847 2015.

848 Garcia, A., Santa-Helena, E., De Falco, A., de Paula Ribeiro, J., Gioda, A., and Gioda, C. R.: Toxicological Effects  
849 of Fine Particulate Matter (PM<sub>2.5</sub>): Health Risks and Associated Systemic Injuries—Systematic Review, *Water,  
850 Air, Soil Pollut.*, 234, 346, <https://doi.org/10.1007/s11270-023-06278-9>, 2023.

851 Garofalo, L. A., Pothier, M. A., Levin, E. J. T., Campos, T., Kreidenweis, S. M., and Farmer, D. K.: Emission and  
852 Evolution of Submicron Organic Aerosol in Smoke from Wildfires in the Western United States, *ACS Earth Sp.  
853 Chem.*, 3, 1237–1247, <https://doi.org/10.1021/acsearthspacechem.9b00125>, 2019.

854 Giglio, L., Schroeder, W., Hall, J., and Justice, C.: MODIS Collection 6 and Collection 6.1 Active Fire Product  
855 User's Guide, Nasa, Version 1., 64, 2021.

856 Gkatzelis, G. I., Coggon, M. M., Stockwell, C. E., Hornbrook, R. S., Allen, H., Apel, E. C., Bela, M. M., Blake, D.  
857 R., Bourgeois, I., Brown, S. S., Campuzano-Jost, P., St. Clair, J. M., Crawford, J. H., Crounse, J. D., Day, D. A.,  
858 DiGangi, J. P., Diskin, G. S., Fried, A., Gilman, J. B., Guo, H., Hair, J. W., Halliday, H. S., Hanisco, T. F., Hannun,  
859 R., Hills, A., Huey, L. G., Jimenez, J. L., Katich, J. M., Lamplugh, A., Lee, Y. R., Liao, J., Lindaas, J., McKeen, S.  
860 A., Mikoviny, T., Nault, B. A., Neuman, J. A., Nowak, J. B., Pagonis, D., Peischl, J., Perring, A. E., Piel, F., Rickly,

861 P. S., Robinson, M. A., Rollins, A. W., Ryerson, T. B., Schueneman, M. K., Schwantes, R. H., Schwarz, J. P.,  
862 Sekimoto, K., Selimovic, V., Shingler, T., Tanner, D. J., Tomsche, L., Vasquez, K. T., Veres, P. R., Washenfelder,  
863 R., Weibring, P., Wennberg, P. O., Wisthaler, A., Wolfe, G. M., Womack, C. C., Xu, L., Ball, K., Yokelson, R. J.,  
864 and Warneke, C.: Parameterizations of US wildfire and prescribed fire emission ratios and emission factors based on  
865 FIREX-AQ aircraft measurements, *Atmos. Chem. Phys.*, 24, 929–956, <https://doi.org/10.5194/acp-24-929-2024>,  
866 2024.

867 Hecobian, A., Zhang, X., Zheng, M., Frank, N., Edgerton, E. S., and Weber, R. J.: Water-soluble organic aerosol  
868 material and the light-absorption characteristics of aqueous extracts measured over the Southeastern United States,  
869 *Atmos. Chem. Phys.*, <https://doi.org/10.5194/acp-10-5965-2010>, 2010.

870 Huang, R., Hu, Y., Russell, A. G., Mulholland, J. A., and Odman, M. T.: The Impacts of Prescribed Fire on PM<sub>2.5</sub>  
871 Air Quality and Human Health: Application to Asthma-Related Emergency Room Visits in Georgia, USA, *Int. J.*  
872 *Environ. Res. Public Health*, 16, 2312, <https://doi.org/10.3390/ijerph16132312>, 2019.

873 Ichoku, C. and Kaufman, Y. J.: A method to derive smoke emission rates from MODIS fire radiative energy  
874 measurements, in: *IEEE Transactions on Geoscience and Remote Sensing*,  
875 <https://doi.org/10.1109/TGRS.2005.857328>, 2005.

876 Jaffe, D. A., O’Neill, S. M., Larkin, N. K., Holder, A. L., Peterson, D. L., Halofsky, J. E., and Rappold, A. G.:  
877 Wildfire and prescribed burning impacts on air quality in the United States,  
878 <https://doi.org/10.1080/10962247.2020.1749731>, 2020.

879 Jaffe, D. A., Schnieder, B., and Inouye, D.: Technical note: Use of PM 2.5 to CO ratio as an indicator of wildfire  
880 smoke in urban areas, *Atmos. Chem. Phys.*, 22, 12695–12704, <https://doi.org/10.5194/acp-22-12695-2022>, 2022.

881 Jo, D. S., Park, R. J., Lee, S., Kim, S. W., and Zhang, X.: A global simulation of brown carbon: Implications for  
882 photochemistry and direct radiative effect, *Atmos. Chem. Phys.*, <https://doi.org/10.5194/acp-16-3413-2016>, 2016.

883 Kelp, M. M., Carroll, M. C., Liu, T., Yantosca, R. M., Hockenberry, H. E., and Mickley, L. J.: Prescribed Burns as a  
884 Tool to Mitigate Future Wildfire Smoke Exposure: Lessons for States and Rural Environmental Justice  
885 Communities, *Earth’s Futur.*, 11, <https://doi.org/10.1029/2022EF003468>, 2023.

886 Korontzi, S., Ward, D. E., Susott, R. A., Yokelson, R. J., Justice, C. O., Hobbs, P. V., Smithwick, E. A. H., and Hao,  
887 W. M.: Seasonal variation and ecosystem dependence of emission factors for selected trace gases and PM 2.5 for  
888 southern African savanna fires, *J. Geophys. Res. Atmos.*, 108, <https://doi.org/10.1029/2003JD003730>, 2003.

889 Kuenzer, C., Hecker, C., Zhang, J., Wessling, S., and Wagner, W.: The potential of multidiurnal MODIS thermal  
890 band data for coal fire detection, *Int. J. Remote Sens.*, <https://doi.org/10.1080/01431160701352147>, 2008.

891 Lack, D. A. and Langridge, J. M.: On the attribution of black and brown carbon light absorption using the Ångström  
892 exponent, *Atmos. Chem. Phys.*, 13, 10535–10543, <https://doi.org/10.5194/acp-13-10535-2013>, 2013.

893 Larkin, N. K., Raffuse, S. M., Huang, S. M., Pavlovic, N., Lahm, P., and Rao, V.: The Comprehensive Fire  
894 Information Reconciled Emissions (CFIRE) inventory: Wildland fire emissions developed for the 2011 and 2014  
895 U.S. National Emissions Inventory, *J. Air Waste Manag. Assoc.*, <https://doi.org/10.1080/10962247.2020.1802365>,  
896 2020.

897 Laskin, A., Laskin, J., and Nizkorodov, S. A.: Chemistry of Atmospheric Brown Carbon, *Chem. Rev.*, 115, 4335–  
898 4382, <https://doi.org/10.1021/cr5006167>, 2015.

899 Lee, J. Y., Daube, C., Fortner, E., Ellsworth, N., May, N. W., Tallant, J., Herndon, S., and Pratt, K. A.: Chemical  
900 characterization of prescribed burn emissions from a mixed forest in Northern Michigan, *Environ. Sci. Atmos.*, 3,  
901 35–48, <https://doi.org/10.1039/D2EA00069E>, 2023.

902 Lee, S., Baumann, K., Schauer, J. J., Sheesley, R. J., Naeher, L. P., Meinardi, S., Blake, D. R., Edgerton, E. S.,  
903 Russell, A. G., and Clements, M.: Gaseous and Particulate Emissions from Prescribed Burning in Georgia, *Environ.*  
904 *Sci. Technol.*, 39, 9049–9056, <https://doi.org/10.1021/es0515831>, 2005.

905 Lee, S., Kim, H. K., Yan, B., Cobb, C. E., Hennigan, C., Nichols, S., Chamber, M., Edgerton, E. S., Jansen, J. J.,  
906 Hu, Y., Zheng, M., Weber, R. J., and Russell, A. G.: Diagnosis of Aged Prescribed Burning Plumes Impacting an  
907 Urban Area, *Environ. Sci. Technol.*, 42, 1438–1444, <https://doi.org/10.1021/es7023059>, 2008.

908 Levy, I., Mihele, C., Lu, G., Narayan, J., Hilker, N., and Brook, J. R.: Elucidating multipollutant exposure across a  
909 complex metropolitan area by systematic deployment of a mobile laboratory, *Atmos. Chem. Phys.*,  
910 <https://doi.org/10.5194/acp-14-7173-2014>, 2014.

911 Li, F., Zhang, X., Kondragunta, S., and Lu, X.: An evaluation of advanced baseline imager fire radiative power  
912 based wildfire emissions using carbon monoxide observed by the Tropospheric Monitoring Instrument across the  
913 conterminous United States, *Environ. Res. Lett.*, 15, 094049, <https://doi.org/10.1088/1748-9326/ab9d3a>, 2020.

914 Liu, D., Zhang, Q., Jiang, J., and Chen, D. R.: Performance calibration of low-cost and portable particular matter  
915 (PM) sensors, *J. Aerosol Sci.*, <https://doi.org/10.1016/j.jaerosci.2017.05.011>, 2017a.

916 Liu, J. C., Pereira, G., Uhl, S. A., Bravo, M. A., and Bell, M. L.: A systematic review of the physical health impacts  
917 from non-occupational exposure to wildfire smoke, *Environ. Res.*, 136, 120–132,  
918 <https://doi.org/10.1016/j.envres.2014.10.015>, 2015.

919 Liu, T., Marlier, M. E., Karambelas, A., Jain, M., Singh, S., Singh, M. K., Gautam, R., and Defries, R. S.: Missing  
920 emissions from post-monsoon agricultural fires in northwestern India: Regional limitations of modis burned area  
921 and active fire products, <https://doi.org/10.1088/2515-7620/ab056c>, 2019.

922 Liu, X., Zhang, Y., Huey, L. G., Yokelson, R. J., Wang, Y., Jimenez, J. L., Campuzano-Jost, P., Beyersdorf, A. J.,  
923 Blake, D. R., Choi, Y., St. Clair, J. M., Crouse, J. D., Day, D. A., Diskin, G. S., Fried, A., Hall, S. R., Hanisco, T.  
924 F., King, L. E., Meinardi, S., Mikoviny, T., Palm, B. B., Peischl, J., Perring, A. E., Pollack, I. B., Ryerson, T. B.,  
925 Sachse, G., Schwarz, J. P., Simpson, I. J., Tanner, D. J., Thornhill, K. L., Ullmann, K., Weber, R. J., Wennberg, P.

926 O., Wisthaler, A., Wolfe, G. M., and Ziemba, L. D.: Agricultural fires in the southeastern U.S. during SEAC4RS:  
927 Emissions of trace gases and particles and evolution of ozone, reactive nitrogen, and organic aerosol, *J. Geophys.*  
928 *Res. Atmos.*, 121, 7383–7414, <https://doi.org/10.1002/2016JD025040>, 2016.

929 Liu, X., Huey, L. G., Yokelson, R. J., Selimovic, V., Simpson, I. J., Müller, M., Jimenez, J. L., Campuzano-Jost, P.,  
930 Beyersdorf, A. J., Blake, D. R., Butterfield, Z., Choi, Y., Crouse, J. D., Day, D. A., Diskin, G. S., Dubey, M. K.,  
931 Fortner, E., Hanisco, T. F., Hu, W., King, L. E., Kleinman, L., Meinardi, S., Mikoviny, T., Onasch, T. B., Palm, B.  
932 B., Peischl, J., Pollack, I. B., Ryerson, T. B., Sachse, G. W., Sedlacek, A. J., Shilling, J. E., Springston, S., St. Clair,  
933 J. M., Tanner, D. J., Teng, A. P., Wennberg, P. O., Wisthaler, A., and Wolfe, G. M.: Airborne measurements of  
934 western U.S. wildfire emissions: Comparison with prescribed burning and air quality implications, *J. Geophys. Res.*  
935 *Atmos.*, 122, 6108–6129, <https://doi.org/10.1002/2016JD026315>, 2017b.

936 Liu, Y., Bourgeois, A., Warner, T., Swerdlin, S., and Hacker, J.: Implementation of observation-nudging based  
937 FDDA into WRF for supporting ATEC test operations, in: In Proceedings of the WRF/MM5 Users' Workshop, 27–  
938 30, 2005.

939 Mallia, D. V., Kochanski, A. K., Urbanski, S. P., Mandel, J., Farguell, A., and Krueger, S. K.: Incorporating a  
940 Canopy Parameterization within a Coupled Fire-Atmosphere Model to Improve a Smoke Simulation for a  
941 Prescribed Burn, *Atmosphere (Basel)*, 11, 832, <https://doi.org/10.3390/atmos11080832>, 2020.

942 Marsavin, A., van Gageldonk, R., Bernays, N., May, N. W., Jaffe, D. A., and Fry, J. L.: Optical properties of  
943 biomass burning aerosol during the 2021 Oregon fire season: comparison between wild and prescribed fires,  
944 *Environ. Sci. Atmos.*, 3, 608–626, <https://doi.org/10.1039/D2EA00118G>, 2023.

945 Martin, M. V., Kahn, R. A., and Tosca, M. G.: A global analysis of wildfire smoke injection heights derived from  
946 space-based multi-angle imaging, *Remote Sens.*, <https://doi.org/10.3390/rs10101609>, 2018.

947 Martinsson, B. G., Friberg, J., Sandvik, O. S., and Sporre, M. K.: Five-satellite-sensor study of the rapid decline of  
948 wildfire smoke in the stratosphere, *Atmos. Chem. Phys.*, <https://doi.org/10.5194/acp-22-3967-2022>, 2022.

949 May, A. A., McMeeking, G. R., Lee, T., Taylor, J. W., Craven, J. S., Burling, I., Sullivan, A. P., Akagi, S., Collett,  
950 J. L., Flynn, M., Coe, H., Urbanski, S. P., Seinfeld, J. H., Yokelson, R. J., and Kreidenweis, S. M.: Aerosol  
951 emissions from prescribed fires in the United States: A synthesis of laboratory and aircraft measurements, *J.*  
952 *Geophys. Res. Atmos.*, 119, 11,826-11,849, <https://doi.org/10.1002/2014JD021848>, 2014.

953 May, A. A., Lee, T., McMeeking, G. R., Akagi, S., Sullivan, A. P., Urbanski, S., Yokelson, R. J., and Kreidenweis,  
954 S. M.: Observations and analysis of organic aerosol evolution in some prescribed fire smoke plumes, *Atmos. Chem.*  
955 *Phys.*, 15, 6323–6335, <https://doi.org/10.5194/acp-15-6323-2015>, 2015.

956 Melvin, M. A.: 2018 National Prescribed Fire Use Report, 2018.

957 Melvin, M. A.: 2020 National Prescribed Fire Use Report, 2020.

958 Melvin, M. A.: 2021 National Prescribed Fire Use Report, 2021.

959 Mildrexler, D. J., Zhao, M., Heinsch, F. A., and Running, S. W.: A new satellite-based methodology for continental-  
960 scale disturbance detection, *Ecol. Appl.*, [https://doi.org/10.1890/1051-0761\(2007\)017\[0235:ANSMFC\]2.0.CO;2](https://doi.org/10.1890/1051-0761(2007)017[0235:ANSMFC]2.0.CO;2),  
961 2007.

962 Naeher, L. P., Brauer, M., Lipsett, M., Zelikoff, J. T., Simpson, C. D., Koenig, J. Q., and Smith, K. R.: Woodsmoke  
963 Health Effects: A Review, *Inhal. Toxicol.*, 19, 67–106, <https://doi.org/10.1080/08958370600985875>, 2007.

964 Nguyen, H. M. and Wooster, M. J.: Advances in the estimation of high Spatio-temporal resolution pan-African top-  
965 down biomass burning emissions made using geostationary fire radiative power (FRP) and MAIAC aerosol optical  
966 depth (AOD) data, *Remote Sens. Environ.*, 248, 111971, <https://doi.org/10.1016/j.rse.2020.111971>, 2020.

967 O’Dell, K., Hornbrook, R. S., Permar, W., Levin, E. J. T., Garofalo, L. A., Apel, E. C., Blake, N. J., Jarnot, A.,  
968 Pothier, M. A., Farmer, D. K., Hu, L., Campos, T., Ford, B., Pierce, J. R., and Fischer, E. V.: Correction to  
969 Hazardous Air Pollutants in Fresh and Aged Western US Wildfire Smoke and Implications for Long-Term  
970 Exposure, *Environ. Sci. Technol.*, 56, 3304–3304, <https://doi.org/10.1021/acs.est.2c01008>, 2022.

971 Pagonis, D., Selimovic, V., Campuzano-Jost, P., Guo, H., Day, D. A., Schueneman, M. K., Nault, B. A., Coggon,  
972 M. M., DiGangi, J. P., Diskin, G. S., Fortner, E. C., Gargulinski, E. M., Gkatzelis, G. I., Hair, J. W., Herndon, S. C.,  
973 Holmes, C. D., Katich, J. M., Nowak, J. B., Perring, A. E., Saide, P., Shingler, T. J., Soja, A. J., Thapa, L. H.,  
974 Warneke, C., Wiggins, E. B., Wisthaler, A., Yacovitch, T. I., Yokelson, R. J., and Jimenez, J. L.: Impact of Biomass  
975 Burning Organic Aerosol Volatility on Smoke Concentrations Downwind of Fires, *Environ. Sci. Technol.*, 57,  
976 17011–17021, <https://doi.org/10.1021/acs.est.3c05017>, 2023.

977 Palm, B. B., Peng, Q., Fredrickson, C. D., Lee, B. H., Garofalo, L. A., Pothier, M. A., Kreidenweis, S. M., Farmer,  
978 D. K., Pokhrel, R. P., Shen, Y., Murphy, S. M., Permar, W., Hu, L., Campos, T. L., Hall, S. R., Ullmann, K., Zhang,  
979 X., Flocke, F., Fischer, E. V., and Thornton, J. A.: Quantification of organic aerosol and brown carbon evolution in  
980 fresh wildfire plumes, *Proc. Natl. Acad. Sci.*, 117, 29469–29477, <https://doi.org/10.1073/pnas.2012218117>, 2020.

981 Parrish, D. D., Holloway, J. S., and Fehsenfeld, F. C.: Routine, Continuous Measurement of Carbon Monoxide with  
982 Parts per Billion Precision, *Environ. Sci. Technol.*, <https://doi.org/10.1021/es00058a013>, 1994.

983 Patashnick, H. and Rupprecht, E. G.: Continuous PM-10 Measurements Using the Tapered Element Oscillating  
984 Microbalance, *J. Air Waste Manage. Assoc.*, 41, 1079–1083, <https://doi.org/10.1080/10473289.1991.10466903>,  
985 1991.

986 Permar, W., Wang, Q., Selimovic, V., Wielgasz, C., Yokelson, R. J., Hornbrook, R. S., Hills, A. J., Apel, E. C., Ku,  
987 I., Zhou, Y., Sive, B. C., Sullivan, A. P., Collett, J. L., Campos, T. L., Palm, B. B., Peng, Q., Thornton, J. A.,  
988 Garofalo, L. A., Farmer, D. K., Kreidenweis, S. M., Levin, E. J. T., DeMott, P. J., Flocke, F., Fischer, E. V., and Hu,  
989 L.: Emissions of Trace Organic Gases From Western U.S. Wildfires Based on WE-CAN Aircraft Measurements, *J.*  
990 *Geophys. Res. Atmos.*, 126, <https://doi.org/10.1029/2020JD033838>, 2021.

991 Pratt, K. A., Murphy, S. M., Subramanian, R., Demott, P. J., Kok, G. L., Campos, T., Rogers, D. C., Prenni, A. J.,  
992 Heymsfield, A. J., Seinfeld, J. H., and Prather, K. A.: Flight-based chemical characterization of biomass burning  
993 aerosols within two prescribed burn smoke plumes, *Atmos. Chem. Phys.*, [https://doi.org/10.5194/acp-11-12549-](https://doi.org/10.5194/acp-11-12549-2011)  
994 2011, 2011.

995 Prichard, S. J., O'Neill, S. M., Eagle, P., Andreu, A. G., Drye, B., Dubowy, J., Urbanski, S., and Strand, T. M.:  
996 Wildland fire emission factors in North America: synthesis of existing data, measurement needs and management  
997 applications, *Int. J. Wildl. Fire*, 29, 132, <https://doi.org/10.1071/WF19066>, 2020.

998 Reid, C. E., Brauer, M., Johnston, F. H., Jerrett, M., Balmes, J. R., and Elliott, C. T.: Critical Review of Health  
999 Impacts of Wildfire Smoke Exposure, *Environ. Health Perspect.*, 124, 1334–1343,  
1000 <https://doi.org/10.1289/ehp.1409277>, 2016.

1001 Saleh, R., Hennigan, C. J., McMeeking, G. R., Chuang, W. K., Robinson, E. S., Coe, H., Donahue, N. M., and  
1002 Robinson, A. L.: Absorptivity of brown carbon in fresh and photo-chemically aged biomass-burning emissions,  
1003 *Atmos. Chem. Phys.*, 13, 7683–7693, <https://doi.org/10.5194/acp-13-7683-2013>, 2013.

1004 Schroeder, W. and Giglio, L.: NASA VIIRS Land Science Investigator Processing System (SIPS) Visible Infrared  
1005 Imaging Radiometer Suite (VIIRS) 375 m & 750 m Active Fire Products: Product User's Guide, Nasa, 1.4, 2–23,  
1006 2018.

1007 Selimovic, V., Yokelson, R. J., McMeeking, G. R., and Coefield, S.: In situ measurements of trace gases, PM, and  
1008 aerosol optical properties during the 2017 NW US wildfire smoke event, *Atmos. Chem. Phys.*, 19, 3905–3926,  
1009 <https://doi.org/10.5194/acp-19-3905-2019>, 2019.

1010 Shamarock, W. C., Klemp, J. B., Dudhia, J., Gill, D. O., Liu, Z., Berner, J., Wang, W., Powers, J. G., Duda, M. G.,  
1011 Barker, D. M., and Huang, X.-Y.: A Description of the Advanced Research WRF Model Version 4,  
1012 <https://doi.org/10.5065/1DFH-6P97>, 2019.

1013 Singleton, M. P., Thode, A. E., Sánchez Meador, A. J., and Iniguez, J. M.: Increasing trends in high-severity fire in  
1014 the southwestern USA from 1984 to 2015, *For. Ecol. Manage.*, 433, 709–719,  
1015 <https://doi.org/10.1016/j.foreco.2018.11.039>, 2019.

1016 Sinha, P., Hobbs, P. V., Yokelson, R. J., Bertschi, I. T., Blake, D. R., Simpson, I. J., Gao, S., Kirchstetter, T. W., and  
1017 Novakov, T.: Emissions of trace gases and particles from savanna fires in southern Africa, *J. Geophys. Res. Atmos.*,  
1018 108, <https://doi.org/10.1029/2002JD002325>, 2003.

1019 Stein, A. F., Draxler, R. R., Rolph, G. D., Stunder, B. J. B., Cohen, M. D., and Ngan, F.: NOAA's HYSPLIT  
1020 Atmospheric Transport and Dispersion Modeling System, *Bull. Am. Meteorol. Soc.*, 96, 2059–2077,  
1021 <https://doi.org/10.1175/BAMS-D-14-00110.1>, 2015.

1022 Strand, T., Gullett, B., Urbanski, S., O'Neill, S., Potter, B., Aurell, J., Holder, A., Larkin, N., Moore, M., and Rorig,  
1023 M.: Grassland and forest understorey biomass emissions from prescribed fires in the south-eastern United States -

- 1024 RxCADRE 2012, *Int. J. Wildl. Fire*, <https://doi.org/10.1071/WF14166>, 2016.
- 1025 Sullivan, A. P., Pokhrel, R. P., Shen, Y., Murphy, S. M., Toohey, D. W., Campos, T., Lindaas, J., Fischer, E. V., and  
1026 Collett Jr., J. L.: Examination of brown carbon absorption from wildfires in the western US during the WE-CAN  
1027 study, *Atmos. Chem. Phys.*, 22, 13389–13406, <https://doi.org/10.5194/acp-22-13389-2022>, 2022.
- 1028 Travis, K. R., Crawford, J. H., Soja, A. J., Gargulinski, E. M., Moore, R. H., Wiggins, E. B., Diskin, G. S., DiGangi,  
1029 J. P., Nowak, J. B., Halliday, H., Yokelson, R. J., McCarty, J. L., Simpson, I. J., Blake, D. R., Meinardi, S.,  
1030 Hornbrook, R. S., Apel, E. C., Hills, A. J., Warneke, C., Coggon, M. M., Rollins, A. W., Gilman, J. B., Womack, C.  
1031 C., Robinson, M. A., Katich, J. M., Peischl, J., Gkatzelis, G. I., Bourgeois, I., Rickly, P. S., Lamplugh, A., Dibb, J.  
1032 E., Jimenez, J. L., Campuzano-Jost, P., Day, D. A., Guo, H., Pagonis, D., Wennberg, P. O., Crounse, J. D., Xu, L.,  
1033 Hanisco, T. F., Wolfe, G. M., Liao, J., St. Clair, J. M., Nault, B. A., Fried, A., and Perring, A. E.: Emission Factors  
1034 for Crop Residue and Prescribed Fires in the Eastern US During FIREX-AQ, *J. Geophys. Res. Atmos.*, 128,  
1035 <https://doi.org/10.1029/2023JD039309>, 2023.
- 1036 USDA: Wildfire crisis strategy implementation plan: A 10-year implementation plan, 1–11, 2022.
- 1037 Virkkula, A., Ahlquist, N. C., Covert, D. S., Arnott, W. P., Sheridan, P. J., Quinn, P. K., and Coffman, D. J.:  
1038 Modification, calibration and a field test of an instrument for measuring light absorption by particles, *Aerosol Sci.*  
1039 *Technol.*, <https://doi.org/10.1080/027868290901963>, 2005.
- 1040 Virkkula, A., Mäkelä, T., Hillamo, R., Yli-Tuomi, T., Hirsikko, A., Hämeri, K., and Koponen, I. K.: A Simple  
1041 Procedure for Correcting Loading Effects of Aethalometer Data, *J. Air Waste Manage. Assoc.*, 57, 1214–1222,  
1042 <https://doi.org/10.3155/1047-3289.57.10.1214>, 2007.
- 1043 Wang, J., Yue, Y., Wang, Y., Ichoku, C., Ellison, L., and Zeng, J.: Mitigating Satellite-Based Fire Sampling  
1044 Limitations in Deriving Biomass Burning Emission Rates: Application to WRF-Chem Model Over the Northern  
1045 sub-Saharan African Region, *J. Geophys. Res. Atmos.*, <https://doi.org/10.1002/2017JD026840>, 2018.
- 1046 Warneke, C., Schwarz, J. P., Dibb, J., Kalashnikova, O., Frost, G., Al-Saad, J., Brown, S. S., Brewer, W. A., Soja,  
1047 A., Seidel, F. C., Washenfelder, R. A., Wiggins, E. B., Moore, R. H., Anderson, B. E., Jordan, C., Yacovitch, T. I.,  
1048 Herndon, S. C., Liu, S., Kuwayama, T., Jaffe, D., Johnston, N., Selimovic, V., Yokelson, R., Giles, D. M., Holben,  
1049 B. N., Goloub, P., Popovici, I., Trainer, M., Kumar, A., Pierce, R. B., Fahey, D., Roberts, J., Gargulinski, E. M.,  
1050 Peterson, D. A., Ye, X., Thapa, L. H., Saide, P. E., Fite, C. H., Holmes, C. D., Wang, S., Coggon, M. M., Decker, Z.  
1051 C. J., Stockwell, C. E., Xu, L., Gkatzelis, G., Aikin, K., Lefer, B., Kaspari, J., Griffin, D., Zeng, L., Weber, R.,  
1052 Hastings, M., Chai, J., Wolfe, G. M., Hanisco, T. F., Liao, J., Campuzano Jost, P., Guo, H., Jimenez, J. L., and  
1053 Crawford, J.: Fire Influence on Regional to Global Environments and Air Quality (FIREX-AQ), *J. Geophys. Res.*  
1054 *Atmos.*, 128, <https://doi.org/10.1029/2022JD037758>, 2023.
- 1055 Wyden, R. and Manchin, J.: National Prescribed Fire Act of 2020, , 116TH CONGRESS. 2D SESSION, 2020.
- 1056 Xi, Y., Kshirsagar, A. V., Wade, T. J., Richardson, D. B., Brookhart, M. A., Wyatt, L., and Rappold, A. G.:



1057 Mortality in US Hemodialysis Patients Following Exposure to Wildfire Smoke, *J. Am. Soc. Nephrol.*, 31, 1824–  
1058 1835, <https://doi.org/10.1681/ASN.2019101066>, 2020.

1059 Xiu, M., Jayaratne, R., Thai, P., Christensen, B., Zing, I., Liu, X., and Morawska, L.: Evaluating the applicability of  
1060 the ratio of PM<sub>2.5</sub> and carbon monoxide as source signatures, *Environ. Pollut.*, 306, 119278,  
1061 <https://doi.org/10.1016/j.envpol.2022.119278>, 2022.

1062 Yan, J., Wang, X., Gong, P., Wang, C., and Cong, Z.: Review of brown carbon aerosols: Recent progress and  
1063 perspectives, *Sci. Total Environ.*, 634, 1475–1485, <https://doi.org/10.1016/j.scitotenv.2018.04.083>, 2018.

1064 Yokelson, R. J., Goode, J. G., Ward, D. E., Susott, R. A., Babbitt, R. E., Wade, D. D., Bertschi, I., Griffith, D. W.  
1065 T., and Hao, W. M.: Emissions of formaldehyde, acetic acid, methanol, and other trace gases from biomass fires in  
1066 North Carolina measured by airborne Fourier transform infrared spectroscopy, *J. Geophys. Res. Atmos.*, 104,  
1067 30109–30125, <https://doi.org/10.1029/1999JD900817>, 1999.

1068 Yokelson, R. J., Burling, I. R., Gilman, J. B., Warneke, C., Stockwell, C. E., De Gouw, J., Akagi, S. K., Urbanski, S.  
1069 P., Veres, P., Roberts, J. M., Kuster, W. C., Reardon, J., Griffith, D. W. T., Johnson, T. J., Hosseini, S., Miller, J.  
1070 W., Cocker, D. R., Jung, H., and Weise, D. R.: Coupling field and laboratory measurements to estimate the emission  
1071 factors of identified and unidentified trace gases for prescribed fires, *Atmos. Chem. Phys.*,  
1072 <https://doi.org/10.5194/acp-13-89-2013>, 2013.

1073 Yu, Y., Zou, W., Jerrett, M., and Meng, Y.-Y.: Acute health impact of wildfire-related and conventional PM<sub>2.5</sub> in  
1074 the United States: A narrative review, *Environ. Adv.*, 12, 100179, <https://doi.org/10.1016/j.envadv.2022.100179>,  
1075 2023.

1076 Zeng, L., Dibb, J., Scheuer, E., Katich, J. M., Schwarz, J. P., Bourgeois, I., Peischl, J., Ryerson, T., Warneke, C.,  
1077 Perring, A. E., Diskin, G. S., DiGangi, J. P., Nowak, J. B., Moore, R. H., Wiggins, E. B., Pagonis, D., Guo, H.,  
1078 Campuzano-Jost, P., Jimenez, J. L., Xu, L., and Weber, R. J.: Characteristics and evolution of brown carbon in  
1079 western United States wildfires, *Atmos. Chem. Phys.*, 22, 8009–8036, <https://doi.org/10.5194/acp-22-8009-2022>,  
1080 2022.

1081 Zhong, M. and Jang, M.: Dynamic light absorption of biomass-burning organic carbon photochemically aged under  
1082 natural sunlight, *Atmos. Chem. Phys.*, 14, 1517–1525, <https://doi.org/10.5194/acp-14-1517-2014>, 2014.

1083

1084

1085 **Tables**

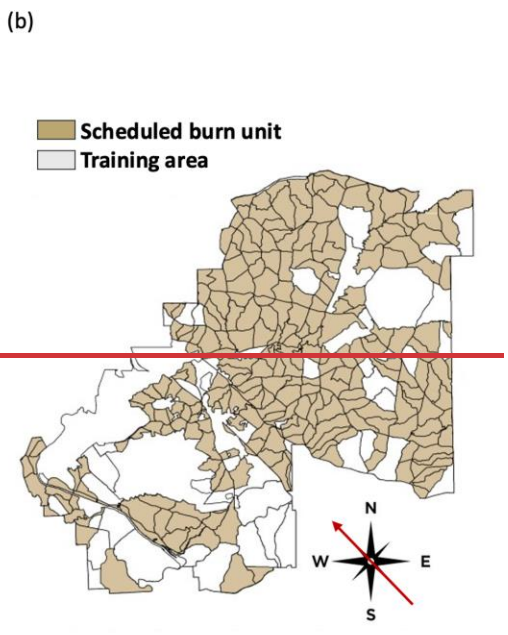
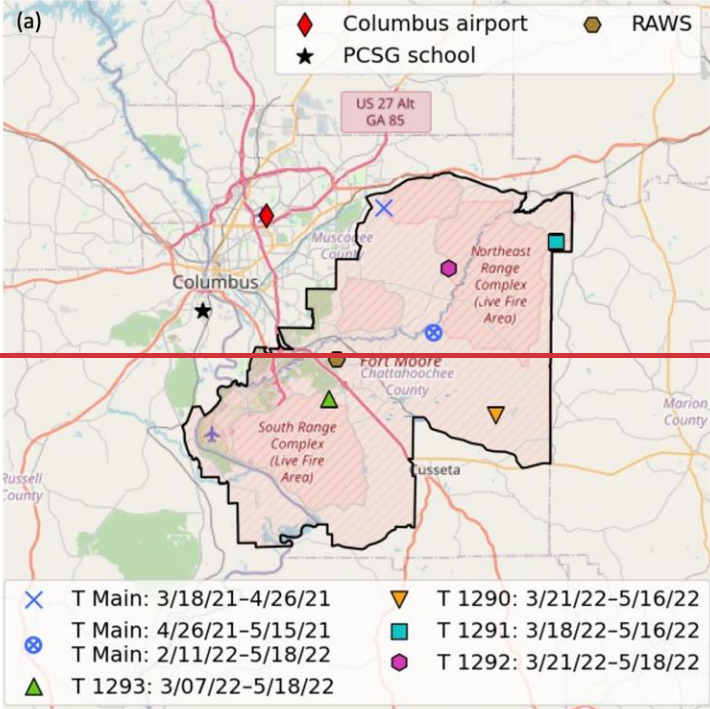
1086 **Table 1.** The PM<sub>2.5</sub> mass, BC, and BrC NEMRs relative to CO (based on regression slopes) and correlation values  
 1087 ( $r^2$ ) in the column to the right of each NEMR for the smoke events identified in this study\*.

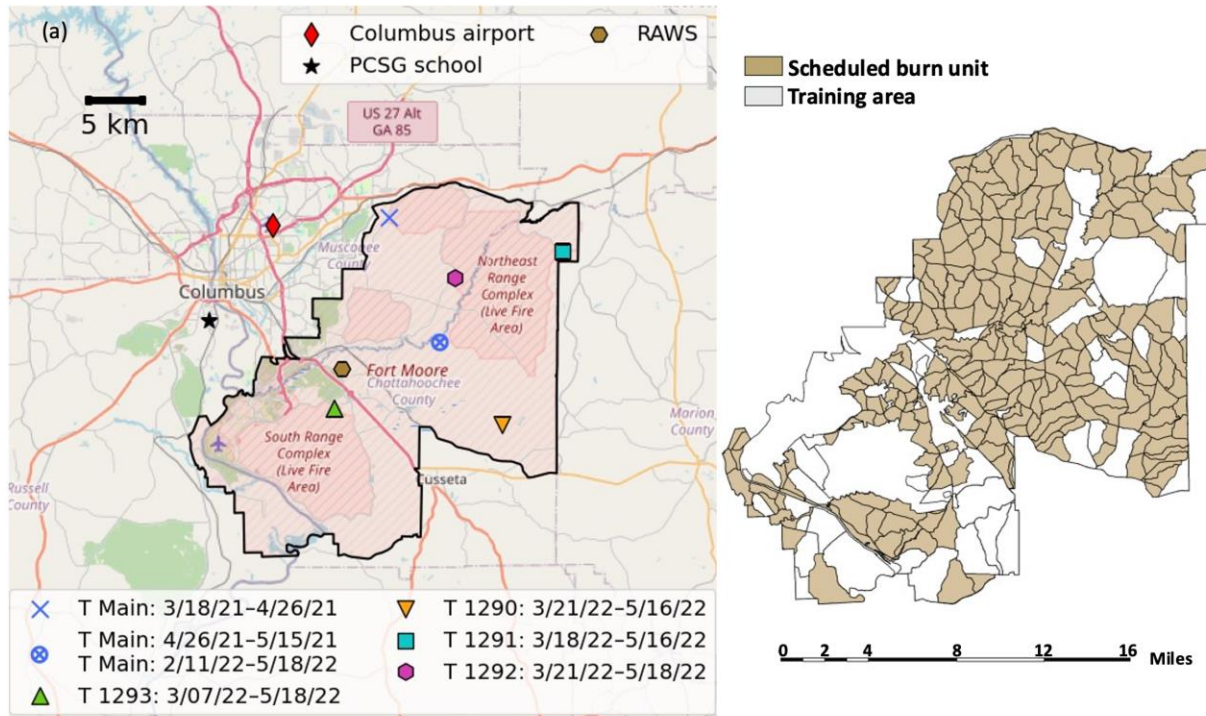
Smoke event Date/Trailer	NEMR PM <sub>2.5</sub> mass ( $\mu\text{g m}^{-3} \text{ppb}^{-1}$ )	$r^2$	NEMR PM <sub>2.5</sub> BC ( $\mu\text{g m}^{-3} \text{ppb}^{-1}$ )	$r^2$	NEMR PM <sub>2.5</sub> BrC ( $\mu\text{g m}^{-3} \text{Mm}^{-1}$ )	$r^2$	Age estimated by wind vector (min)	Age estimated by HYSPLIT (min)
3/23/21 T Main	0.125	0.66	0.010	0.74	0.257	0.59	108	40
4/06/21 T Main	0.097	0.90	0.012	0.96	0.187	0.82	75	130
4/07/21 T Main	0.160	0.90	0.012	0.93	0.367	0.86	14	10
4/08/21 T Main	0.105	0.90	0.005	0.84	0.199	0.85	162	40
4/14/21 T Main	0.146	0.72	0.015	0.76	0.324	0.61	44	20
4/20/21 T Main	0.080	0.74	0.011	0.83	0.151	0.63	5	10
4/21/21 T Main	0.107	0.75	0.009	0.90	0.133	0.70	330	190
4/30/21 T Main	0.141	0.94	0.007	0.95	0.319	0.87	-	-
2/11/22 T Main	0.054	0.93	0.022	0.95	0.567	0.95	8	10
2/12/22 T Main	0.066	0.82	0.018	0.96	0.514	0.93	60	50
2/13/22 T Main	0.053	0.81	0.016	0.83	0.613	0.85	26	20
2/13/22 T Main	0.042	0.86	0.014	0.89	0.689	0.85	30	20
2/26/22 T Main	0.207	0.88	0.018	0.98	0.690	0.97	130	110
2/27/22 T Main	0.119	0.70	0.010	0.87	0.334	0.91	-	-
3/01/22 T Main	0.166	0.81	0.016	0.91	0.586	0.94	92	270
3/02/22 T Main	0.129	0.75	0.020	0.87	0.608	0.87	60	40
3/04/22 T Main	0.209	0.69	0.005	0.53	0.167	0.92	-	160
3/04/22 T Main	0.121	0.89	0.012	0.98	0.454	0.97	-	40
3/07/22 T Main	0.122	0.82	0.009	0.96	0.405	0.96	224	-
3/07/22 T Main	0.170	0.66	0.012	0.97	0.338	0.89	-	10
3/14/22 T Main	0.138	0.82	0.010	0.93	0.575	0.88	-	20
3/25/22 T Main	0.090	0.78	0.009	0.86	0.375	0.91	5	10
3/29/22 T Main	0.121	0.68	0.008	0.68	0.420	0.76	5	10
4/04/22 T Main	0.129	0.90	0.009	0.96	0.551	0.92	168	130
4/25/22 T Main	0.283	0.83	0.022	0.91	1.382	0.77	169	90
5/09/22 T Main	0.237	0.96	0.008	0.94	0.324	0.94	330	150
3/21/22 T 1293	0.188	0.98	-	-	-	-	89	20
3/25/22 T 1293	0.158	0.93	-	-	-	-	45	30
3/26/22 T 1293	0.148	0.97	-	-	-	-	5	10
3/27/22 T 1293	0.176	0.84	-	-	-	-	5	10
3/28/22 T 1293	0.129	0.81	-	-	-	-	-	60
3/29/22 T 1293	0.093	0.87	-	-	-	-	-	210
4/05/22 T 1293	0.277	0.91	0.016	0.78	0.280	0.47	-	360
4/21/22 T 1293	0.466	0.98	0.024	0.83	1.55	0.48	78	-
4/23/22 T 1293	0.121	0.59	0.013	0.80	0.317	0.33	28	10
4/23/22 T 1293	0.165	0.97	0.014	0.96	0.354	0.94	48	10
4/24/22 T 1293	0.248	0.90	-	-	-	-	63	40
4/26/22 T 1293	0.182	0.96	-	-	-	-	106	-
5/09/22 T 1293	0.238	0.99	0.012	0.98	0.321	0.94	480	210
5/10/22 T 1293	0.112	0.92	0.008	0.83	0.406	0.78	474	160
5/11/22 T 1293	0.168	0.77	-	-	-	-	5	10
5/12/22 T 1293	0.119	0.94	-	-	-	-	5	10
5/09/22 T 1291	0.265	0.98	-	-	-	-	296	160

1088 \* The table lists all events where both PM<sub>2.5</sub> mass and CO concentration were both available. In some cases BC and  
 1089 BrC data was not available and left as blank values (-).

1090







1093

1094

1095

1096

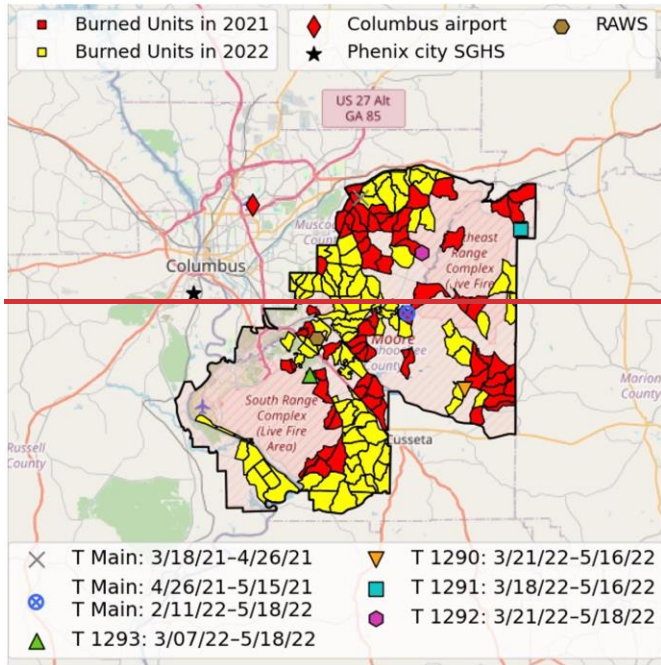
1097

1098

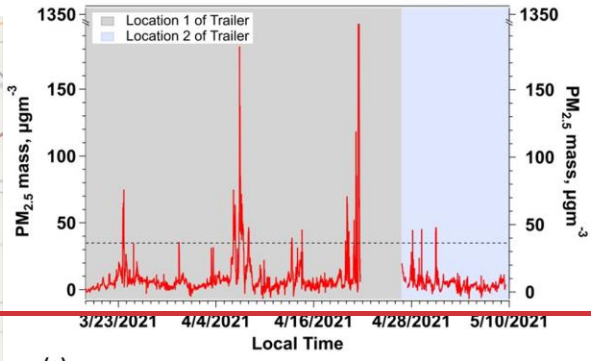
**Figure 1.** Study region overview. (a) Fort Moore map with the locations of trailers, RAWs weather station, and two state-operated sampling sites, Columbus Airport and Phenix City South Girard (PCSG) school, are shown along with the location of the city of Columbus GA. (b) Fort Moore map showing the planned burn units for the year 2021, sourced from Fort Moore authorities and natural resources management team, with prevailing winds in the region.



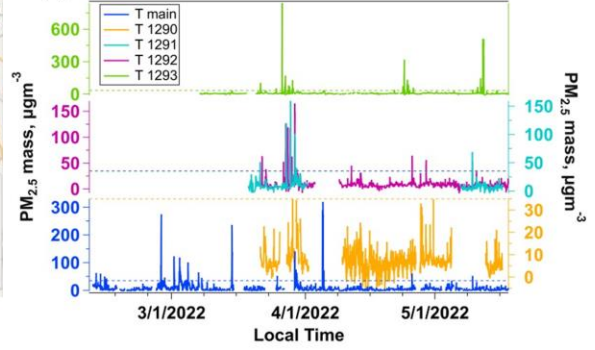
(a)

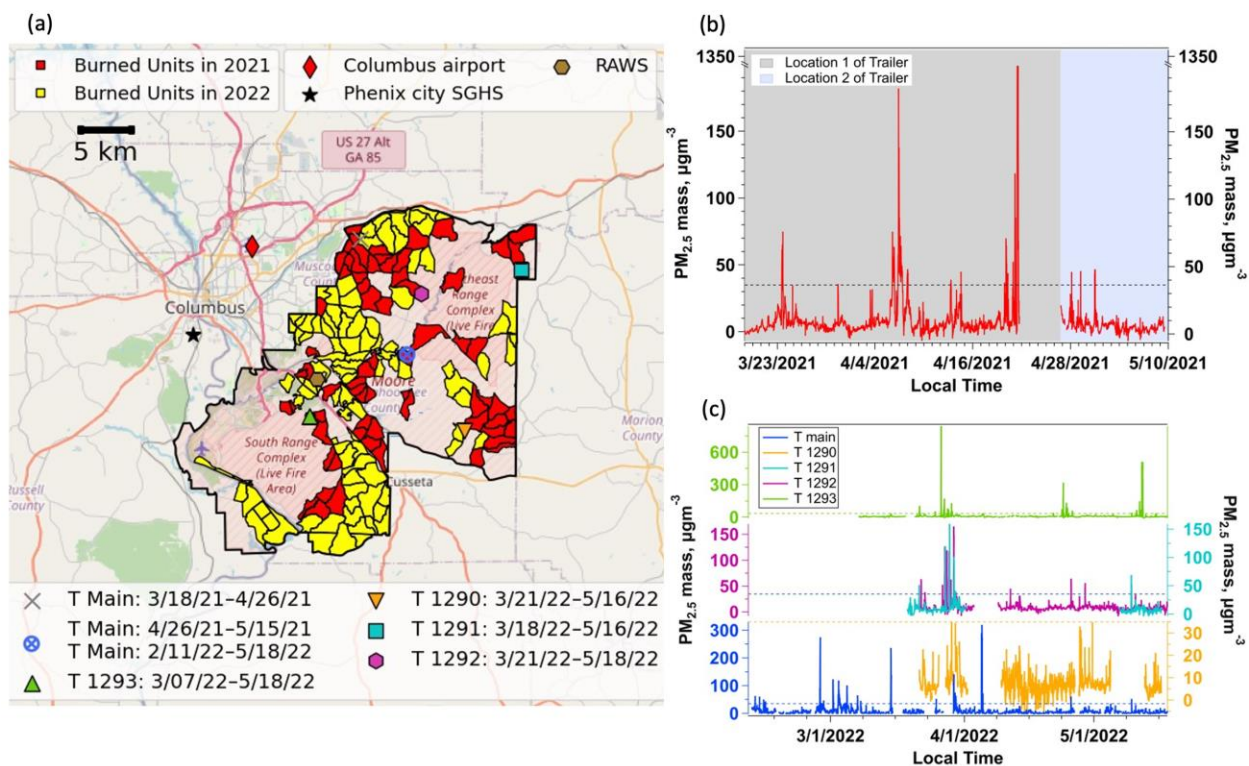


(b)



(c)





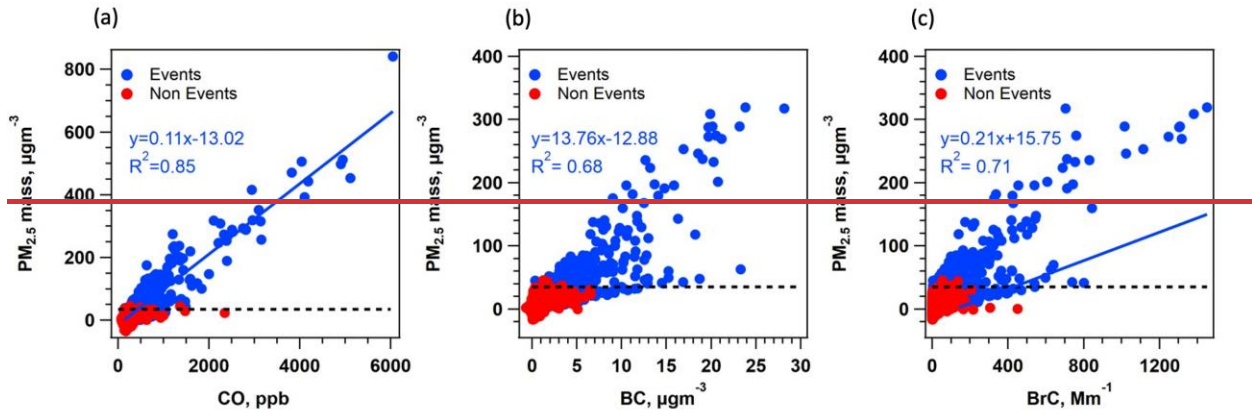
1101

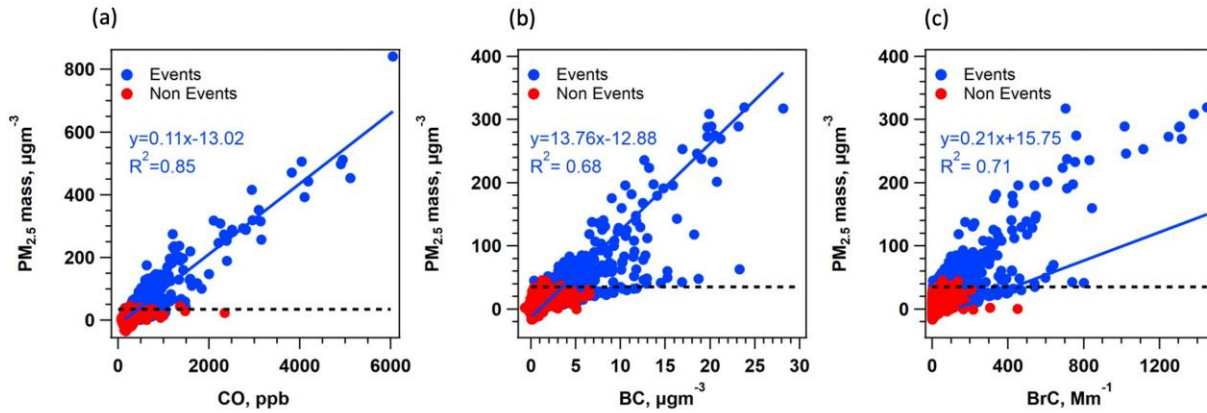
1102 **Figure 2.** PM<sub>2.5</sub> mass measurements over two years study of burning. (a) Map of the burnt areas in the years 2021 and 2022 and  
 1103 locations of monitoring sites. (b) Time series of 20-minute average PM<sub>2.5</sub> mass concentration measured at the main trailer during  
 1104 the burning season of 2021, and (c) 2022 across different sites. Dotted lines represent PM<sub>2.5</sub> mass concentration of 35 μg m<sup>-3</sup>  
 1105 above which peaks were selected for detailed analysis.

1106







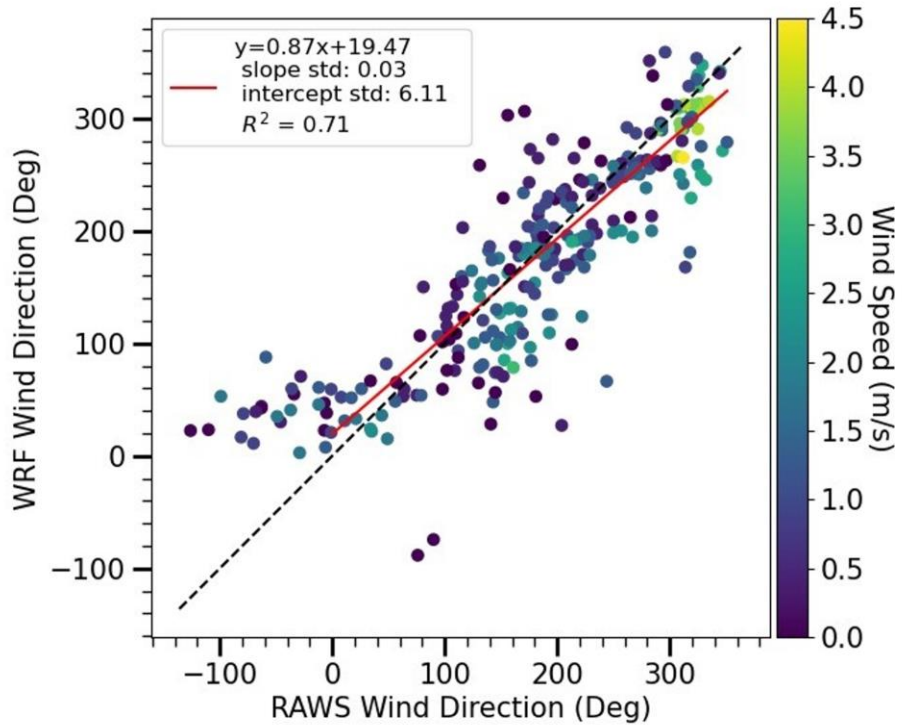


1109

1110 **Figure 3.** Correlations between PM<sub>2.5</sub> mass concentration and CO, PM<sub>2.5</sub> BC and PM<sub>2.5</sub> BrC for measurements from the main  
 1111 trailer in 2021 and 2022 and T1291 and T1293 in 2022. Blue data points are characterized as PM<sub>2.5</sub> events when the concentration  
 1112 is > 35 µg m<sup>-3</sup> averaged over a 20-minute period. In the plot all data associated with an identified event is shown as blue (This  
 1113 includes event data down to the background levels before and after the peak). All other data (non-events) are shown in red. Slope  
 1114 is from orthogonal distance regression (ODR) of the 20-minute averaged data during events periods.

1115

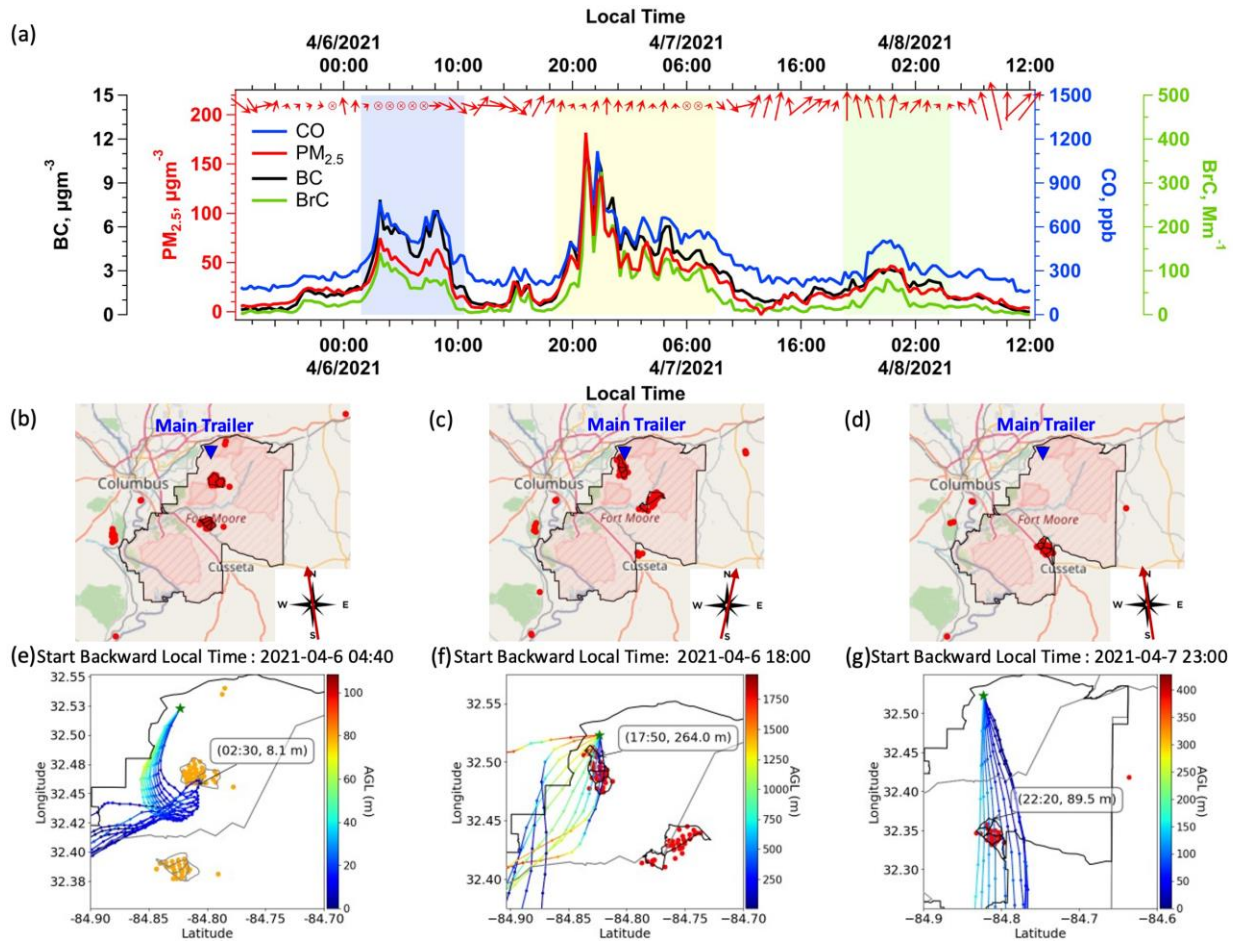
1116



1117

1118 **Figure 4.** Comparison between wind direction modeled via WRF versus that recorded by the RAWS located on Fort Moore.  
1119 Slope is from orthogonal distance regression (ODR).

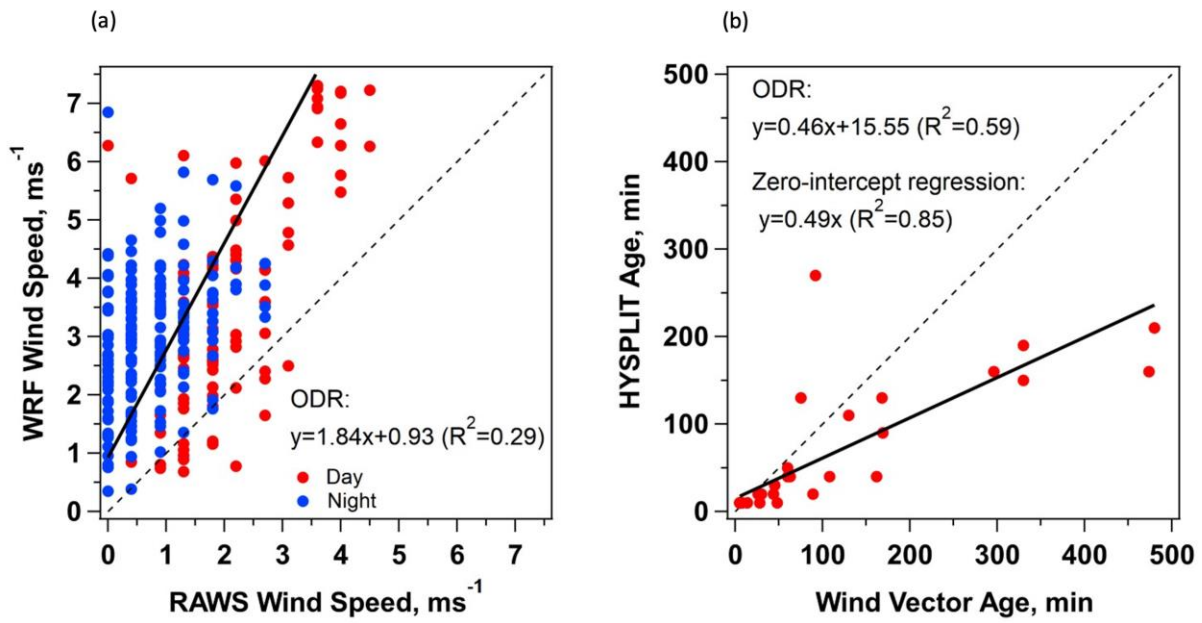
1120



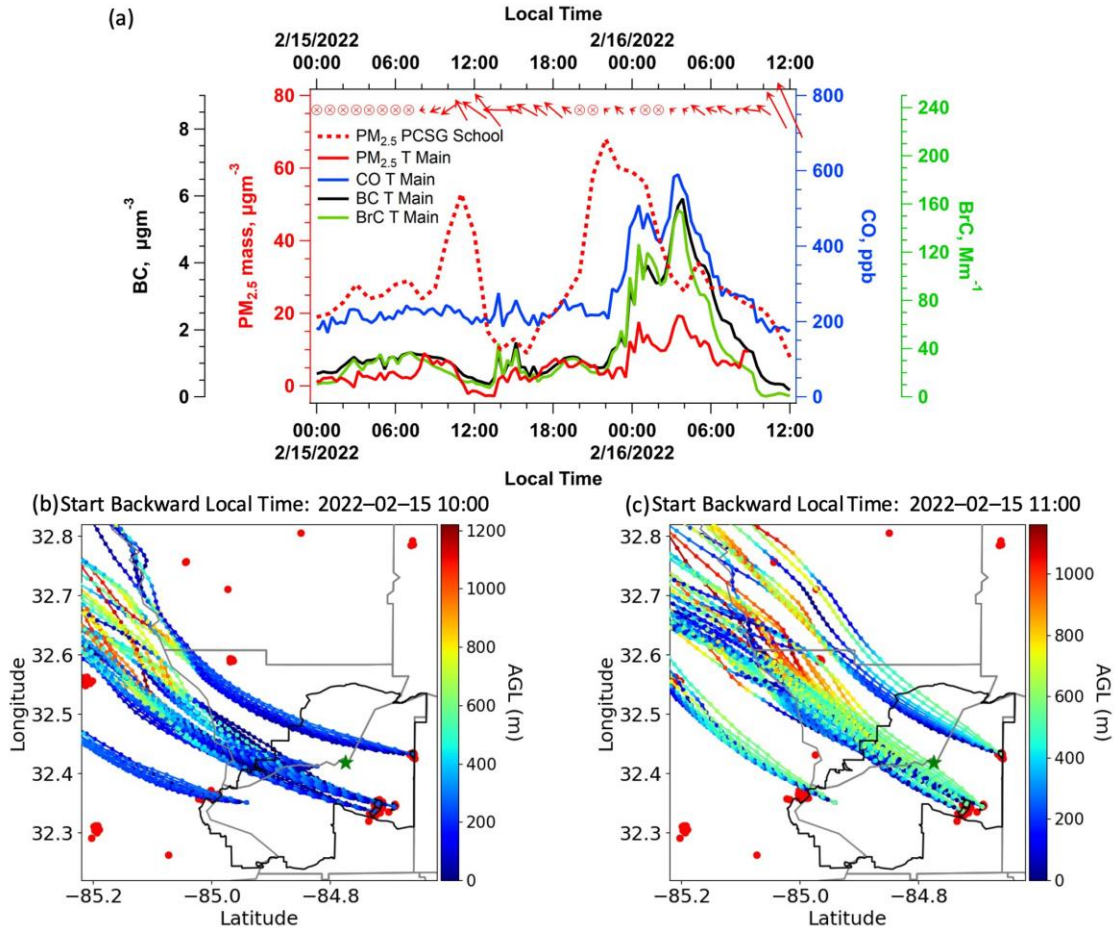
1122

1123 **Figure 5.** Three case studies illustrating the application of our method in determining the source of smoke events. (a) Time\_series  
 1124 of species measured on main trailer. Time resolution is 20 minutes for CO, PM<sub>2.5</sub> mass, BC, and BrC. The wind vectors depict  
 1125 hourly data obtained from RAWS, with the direction of the arrow indicating wind direction, while the length of the arrow  
 1126 represents wind speed. (b,c,d) maps of the Fort showing historical satellite data from the FIRMS website observed for April 5, 6,  
 1127 and 7, 2022. Red dots represent fires detected by the satellite. (e,f,g) are HYSPLIT back trajectories during the occurrence of  
 1128 each of the three peaks. Date and time of the backward trajectory is indicated on top of each map. Time and height at which the  
 1129 trajectory crosses the trailer is shown in the box inside each map. Red dots are fires detected on FIRMS the same day of the  
 1130 backward trajectory. Orange dots are fires detected on FIRMS one day before the day of the backward trajectory. The colors of  
 1131 the scatter are the height above ground level. Green star marks the location of the main trailer. Satellite overpasses times  
 1132 are shown in Table S98.

1133



1136 **Figure 6.** (a) Comparison between wind speed modeled via WRF versus that observed by RAWS located on Fort Moore. (b)  
1137 Comparison between age estimated using HYSPLIT model vs wind vector method.

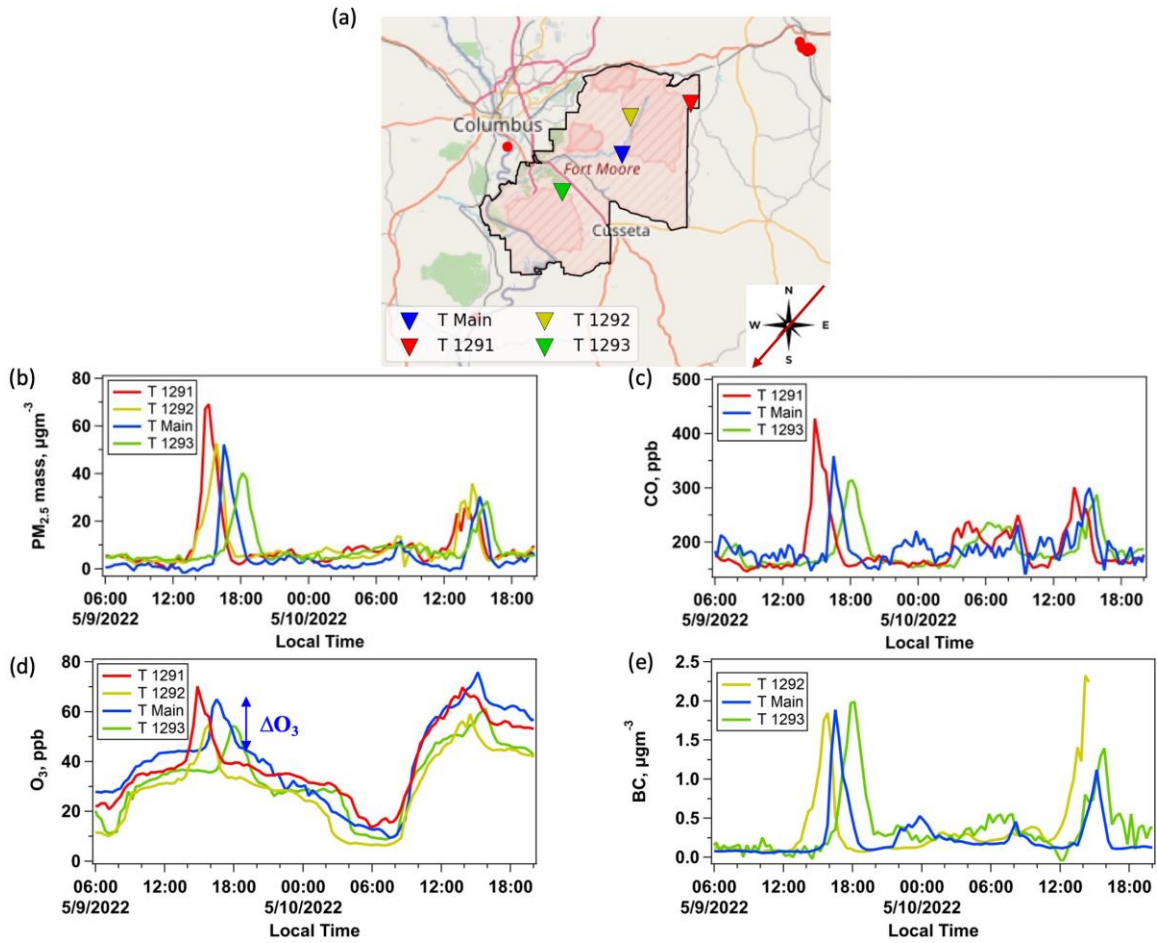


1140

1141  
 1142  
 1143  
 1144  
 1145  
 1146

**Figure 7.** Case study of missing smoke at monitoring site despite expectations according to wind direction. (a) Time series of species measured on main trailer. Time resolution is 20 minutes for CO, PM<sub>2.5</sub> mass, BC, and BrC. The wind vectors depict hourly data sourced from RAWS, with the direction of the arrow indicating wind direction, while the length of the arrow represents wind speed. Data from PCSG school are hourly averages; (b, c) HYSPLIT forward trajectories starting from the two prescribed fires on the base on February 15, 2022 at 10:00 and 11:00, respectively. Red dots are fires detected on FIRMS the same day (satellite overpass happened on February 15, 2022 at 12:54, 13:49, 14:32, and 14:36).

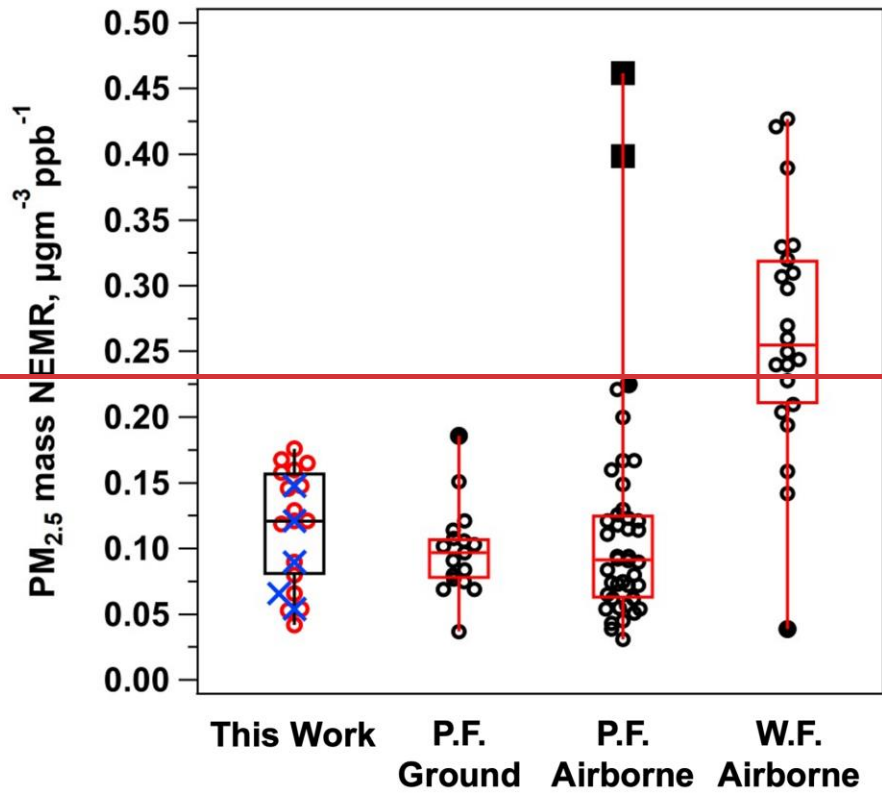
1147



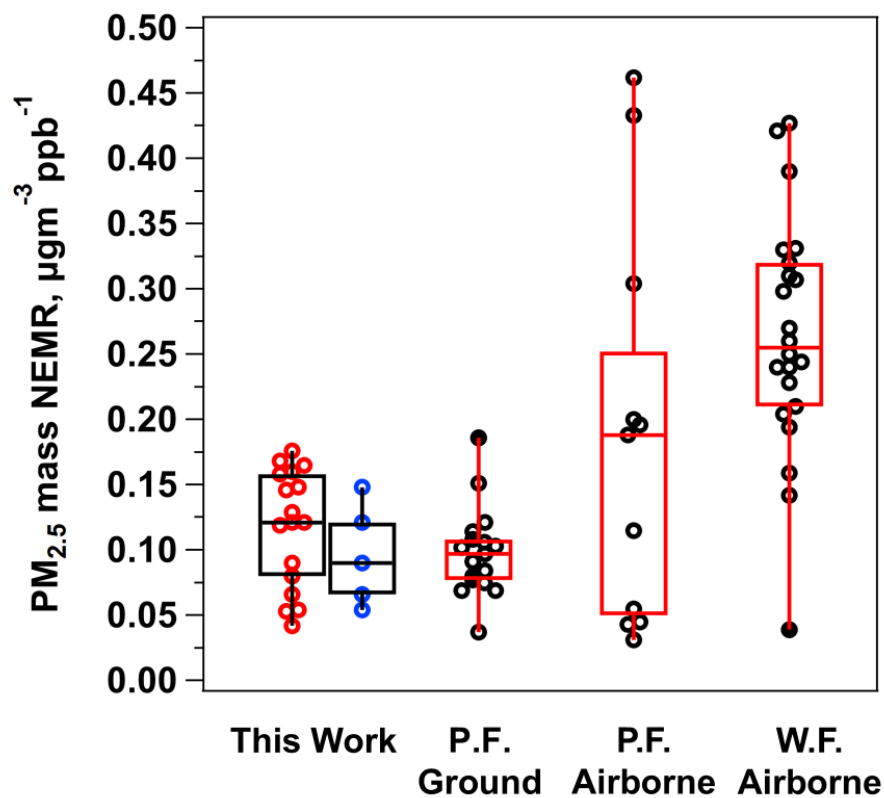
1150 **Figure 8.** Case study of smoke detection sequentially on 4 monitoring trailers. (a) Map of the Fort showing historical satellite  
1151 data from the FIRMS website observed for May 9, 2022 (satellite overpass happened on May 9, 2022 at 12:38, 13:54, and 14:42)  
1152 and average wind vector from 13:00 to 16:00 local time. Time series showing 20 minutes data of (b) PM<sub>2.5</sub> mass and (c) CO on  
1153 main trailer, (d) O<sub>3</sub> concentration, and (e) BC concentration for, main trailer, T1291, T1292, and T1293. Note that no CO  
1154 instrument was operating on T1292 and no BC data for T1291.







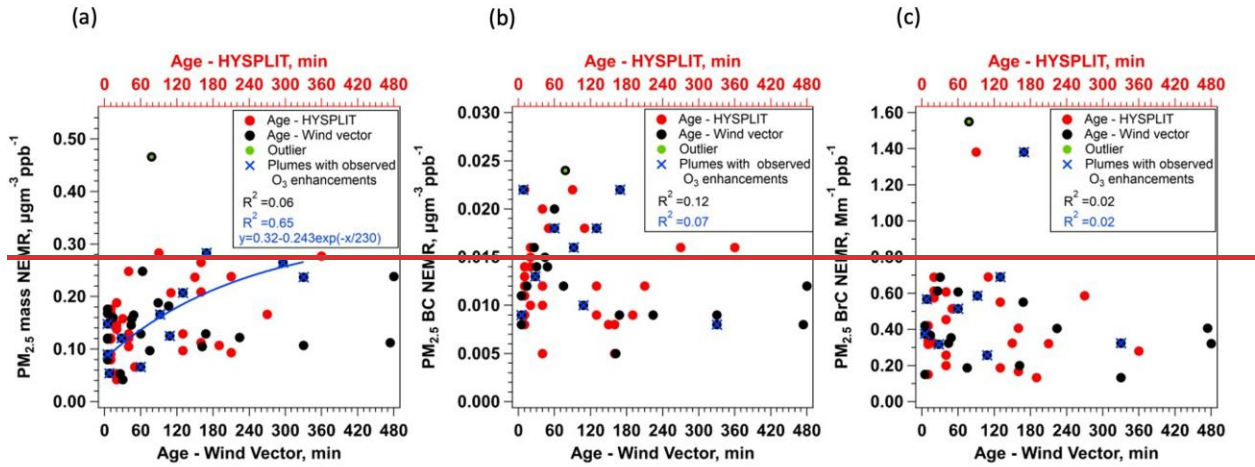
1157

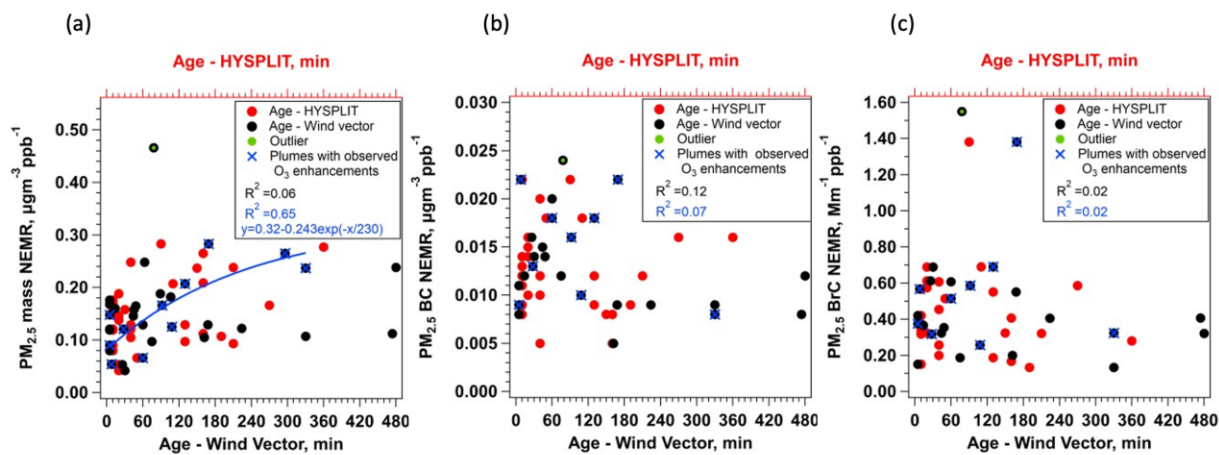


1158

1159 **Figure 9.** Box plot of PM<sub>2.5</sub> mass NEMRs of smoke events of estimated age ≤ 1 hour in this study in comparison to other  
 1160 studies. Blue symbols in This Work are smoke plumes with observed O<sub>3</sub> enhancements. The horizontal line inside the box  
 1161 represents the median of the data. The top line of the box represents the third quartile (Q3), and the bottom line represents  
 1162 the first quartile (Q1). Colored circles and squares represent data outliers and far-outliers respectively. P. F. is Prescribed Fires,  
 1163 W.F. is wildfires. Some of the emission ratios reported in literature and included in the plot corresponds to ΔOA/ΔCO since OA  
 1164 tends to dominate ΔPM<sub>2.5</sub> mass concentration (see Table S10).



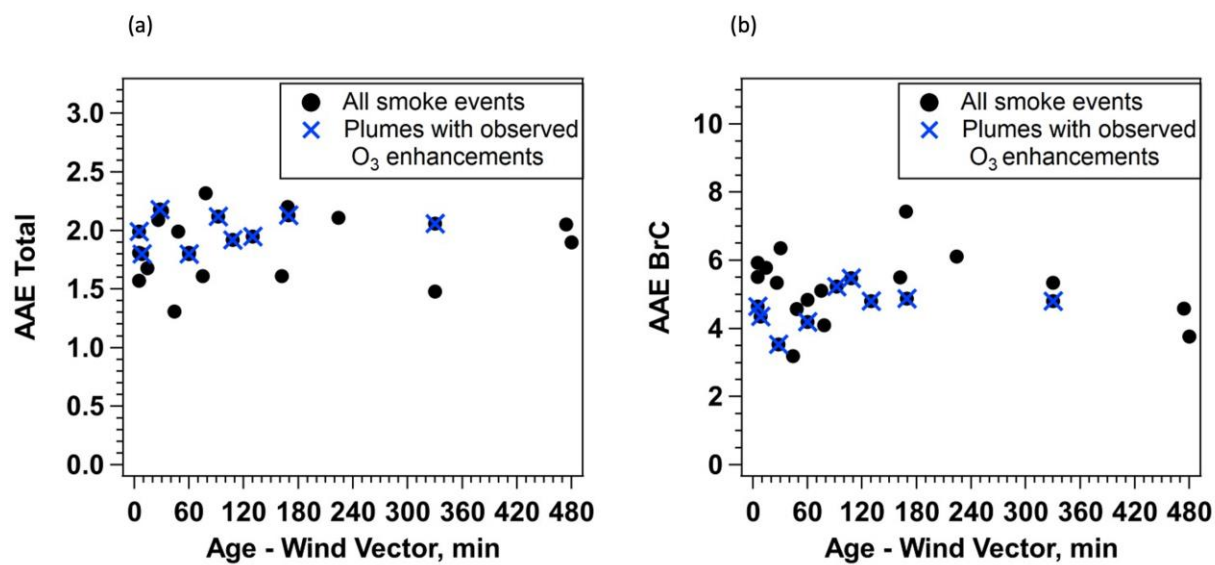




1167

1168 **Figure 10.** (a)  $PM_{2.5}$  mass, (b) BC, and (c) BrC NEMRs of all studied smoke events as a function of age estimated using average  
 1169 wind vector and HYSPLIT analysis. Smoke plumes with observed  $O_3$  enhancements are identified and plotted versus wind vector  
 1170 age. Linear regression coefficients of variation ( $r^2$ ) for all data and for just  $O_3$  enhancement periods are identified. Exponential fit  
 1171 equation for  $PM_{2.5}$  mass NEMRs for  $O_3$  enhancement periods is shown in (a).

1172



1174

1175 **Figure 11.** Average AAE values for a) total (BC+BrC) and b) BrC species for all smoke events of which aethalometer data is  
 1176 available. Smoke plumes with observed O<sub>3</sub> enhancements are identified.

1177

1178

1179

1180

1181

1182